Received: 24 May 2022 | Revised: 3 July 2022 | Accepted: 3 July 2022

DOI: 10.1002/pc.26905

REVIEW ARTICLE

Polymer COMPOSITES WILEY

Scalable methods for directional assembly of fillers in polymer composites: Creating pathways for improving material properties

Anthony Griffin[1] | Yuanhao Guo[2] | Zhendong Hu[3] | Jianming Zhang[3] | Yuwei Chen[3] | Zhe Qiang[1]

[1]School of Polymer Science and Engineering, University of Southern Mississippi, Hattiesburg, Mississippi, USA

[2]Department of Polymer Engineering, University of Akron, Akron, Ohio, USA

[3]Key Laboratory of Rubber-Plastics, Ministry of Education/Shandong Provincial Key Laboratory of Rubber- Plastics, Qingdao University of Science & Technology, Qingdao, China

Correspondence
Yuwei Chen, Key Laboratory of Rubber-Plastics, Ministry of Education/Shandong Provincial Key Laboratory of Rubber-Plastics, Qingdao University of Science & Technology, Qingdao, 266042, China.
Email: yuweichen@qust.edu.cn

Zhe Qiang, School of Polymer Science and Engineering, University of Southern Mississippi, Hattiesburg, MS 39406, USA.
Email: zhe.qiang@usm.edu

Funding information
National Science Foundation Office of Integrative Activities, Grant/Award Number: 1757220

Abstract

Polymer composites are ubiquitous and indispensable in numerous applications. Coupling the inclusion of reinforcing agents with methods developed to control filler distribution and orientation allow for significant enhancement in mechanical, thermal, electrical, and barrier/transport-related properties of composites. For practical implementation, ideal approaches to fabricating polymer composites with directionally assembled fillers must consider manufacturing compatibility, scale-up ease, and aligning efficiency. In this article, we will review a cost-effective and industrially relevant toolbox for preferential filler alignment in polymer composites. Three main strategies for aligning fillers within polymer composites will be discussed. Specifically, solution casting and compression molding can introduce compression force to assemble fillers along the in-plane direction of composite films, shear force can be developed during fiber spinning, film blowing, and uniaxial/biaxial stretching processes to align fillers along the shear direction, and external fields (both electric and magnetic fields) can direct assembly of fillers, typically along the out-of-plane direction. For each section, we not only highlight the mechanisms of these methods but also demonstrate the critical structure–property relationships through model examples. Finally, a perspective on future opportunities and challenges of anisotropic and performance-enhanced polymer composite preparation strategies is provided, with a particular focus on additive manufacturing.

KEYWORDS

functional polymers, nanocomposites, processing, self-assembly, structure-property relations

1 | INTRODUCTION

Polymer composites are multi-component materials, where the inclusion of reinforcing and/or functional agents into a polymer matrix leads to property enhancement.[1,2] The science, technology, and engineering of these composite materials are essential for a wide range of applications, including biomedicine,[3–6] aerospace,[7–12] energy storage,[13–18] water remediation,[19–23] commodity plastics,[24–27] and high-performance coatings.[28–30] Specifically, reinforcing agents (i.e., fillers) enable the attainment of various desired performances in resulting composites,

such as mechanical,[31–34] thermal,[35,36] electrical,[37–39] and barrier/transport-related properties.[40,41] In general, the composite properties are collectively determined by the filler type,[42,43] content,[44,45] and composite morphology (i.e., how the filler is assembled in the matrix).[46,47] While a higher loading of fillers is often beneficial, it is important to recognize that increasing filler loading content can lead to several complications including, but not limited to, processing difficulty due to increased viscosity,[48] particle aggregation with macroscopic inhomogeneity,[49–51] and diminishment of key features from the polymer matrix (e.g., mechanical flexibility and optical transparency).[52–54] Addressing these challenges often requires careful system optimization, which may involve extensive experiments and investigations to fully understand the trade-offs between distinct material properties as a function of filler content. Early work in the field of polymer composites for controlling the distribution of fillers often employed several methods to create homogeneous dispersion of fillers in the matrix, such as sonication,[55,56] mixing,[57–59] and high shearing.[60,61] Building on these efforts, it was found that controlling filler distribution is advantageous for enhancing composite properties in many practical applications,[62–66] particularly through developing interconnected (network-like) or macroscopically oriented filler morphology. For example, aligning reinforcing agents in the polymer matrix along the thickness direction can improve the ability of composites to withstand external force,[63,67,68] through effective dissipation of locally concentrated energy.[69,70] Additionally, filler alignment can create directional transport channels for facilitating the diffusion of thermal energy,[71,72] electrons,[73,74] and/or guest molecules,[75–77] leading to significant improvements in material performance compared to their randomly oriented analogues.[78–80] Therefore, development of polymer composites with oriented filler particles is important for many applications such as dielectric sensors/capacitors,[81–84] water purification,[85,86] energy storage,[87–89] and thermal management.[90–93]

Directional assembly of fillers within the polymer matrix can be achieved through several strategies, including the use of compression force,[94,95] shearing,[96–99] and external fields,[100,101] which are applicable at an industrial scale. Specifically, compression force can be introduced through compression molding[94] or controlled solvent evaporation,[95,102] where embedded particles are oriented parallel to the in-plane direction of a composite film. Several conventional polymer processing techniques, including fiber spinning,[97] film blowing,[98] and uniaxial stretching,[103] can be employed to introduce sufficient mechanical force for orienting fillers within the composite. Shearing is also involved in injection molding,[104–107] plate shearing,[108] and roll-milling,[109–111] which can provide an alternative mechanism to develop directional assembly of particles in the polymer matrix. Additionally, application of external fields can polarize fillers, resulting in their alignment within a matrix along the field direction. This article primarily focuses on discussing these cost-effective and industrially relevant methods for aligning fillers along preferential directions in polymer composites. We will discuss the fundamentals and applications of different methods and the resulting structure–property relationship using model examples. The primary goal of this review is to provide readers sufficient working knowledge for understanding the corresponding mechanisms and conducting related experimental investigations. Furthermore, a brief perspective on the future opportunities and challenges in this exciting research arena will be provided.

2 | COMPRESSION FORCE

2.1 | Solution casting

Solution casting, including spin-coating,[112,113] blade-coating,[114–116] and dip-coating,[117–119] is a common processing technique for manufacturing polymer composites. These methods typically involve deposition of polymer solutions onto a substrate followed by solvent evaporation. Upon film drying, polymer composites experience one dimensional shrinkage along the thickness direction due to the removal of volatile solvents.[120] During this process, in-plane stress can be developed from the constrained volume shrinkage, leading to the effective "lay-down" of polymer chains as well as fillers in the direction that is parallel to the film surface.[121] In general, developing such planar orientation of particles with flaky (or other 2D) morphology in polymer composites is useful for enhancing their gas/liquid barrier properties,[122] improving in-plane thermal and electrical conductivity,[123] and enabling controlled drug release/delivery behaviors.[124]

Previous studies have demonstrated that parallel orientation of clay platelets from solvent evaporation can result in a substantial decrease in gas permeability of polymer composites, observed with oxygen,[125] carbon dioxide,[126] helium,[127] and nitrogen molecules.[128] For example, tamarind seed xyloglucan/clay (montmorillonite, or MTM) nanocomposite films can be prepared by casting the water suspension on Teflon molds, followed by a drying step at 40°C overnight.[129] The cross-sectional scanning electron microscopy (SEM) image of the resulting film (Figure 1A) displayed a nearly perfect in-plane orientation of embedded clay platelets, which was consistent with X-ray diffraction (XRD) results showing the transformation from a circular diffraction pattern to two sharp arches upon solvent drying (Figure 1B).

The XRD pattern (Figure 1C) perpendicular to the film surface indicated the random orientation of fillers within the in-plane direction of films. The planar orientation of clay platelets and their intercalated structures in the composite was also confirmed by the transmission electron microscopy (TEM) image, as shown in Figure 1D. The drying induced orientation of clay nanoplatelets resulted in a remarkable enhancement of gas barrier properties; a reduction of oxygen permeability of more than 90% was achieved with only 5 wt% clay platelets (Figure 1E). Specifically, highly oriented clay platelets led to gas molecules encountering a Zigzag tortuous path throughout the thickness direction of the films. In another study, the kinetics of solvent evaporation-induced orientation of polymer chains and graphene oxide nanosheets were investigated via measuring real-time birefringence change of polyamide-imide (PAI)/graphene oxide (GO) nanosheets.[130] The development of out-of-plane optical birefringence confirms the parallel orientation of both polymer chains and GO nanosheets upon the evaporation of dimethylacetamide (DMAc). The planar orientation of GO nanosheets led to an approximately 35% reduction in oxygen permeability for films with only 0.01 wt% of fillers. This result clearly indicated that developing in-plane aligned fillers can hinder gas diffusion in composites. Similarly, Giannelis et al. observed that the parallel orientation of clay nanoparticles in Nafion nanocomposite membranes, resulted from solution casting of a water suspension at 180°C, reduced liquid methanol permeability by almost 90% when the filler content was only 4 vol%.[131]

Moreover, Kim et al. found that graphene oxide (GO) platelets can be self-assembled and oriented in parallel to the surface of polyurethane (PU) films after water evaporation,[132] which was confirmed by cross-sectional SEM imaging. It was found that when GO platelet content was above a threshold value (2%), their alignment was significantly enhanced as steric hindrance between GO platelets promoted rearrangement and overlapping due to entropy maximization. Additionally, highly aligned GO platelets within composites can be in-situ reduced through exposure to hydrazine, resulting in reduced GO (rGO) to further improve the composite functionality. These oriented rGO sheets (with 0.5 wt% loading content) resulted in significantly enhanced electrical conductivity (from $\sim 10^{-11}$ to $\sim 10^{-6}$ S/cm) of final composites. As the content of rGO further increased to 2 wt%, the electrical conductivity of composite improved to 0.09 S/cm, approximately 10 orders of magnitude improvement compared to the pure PU films.

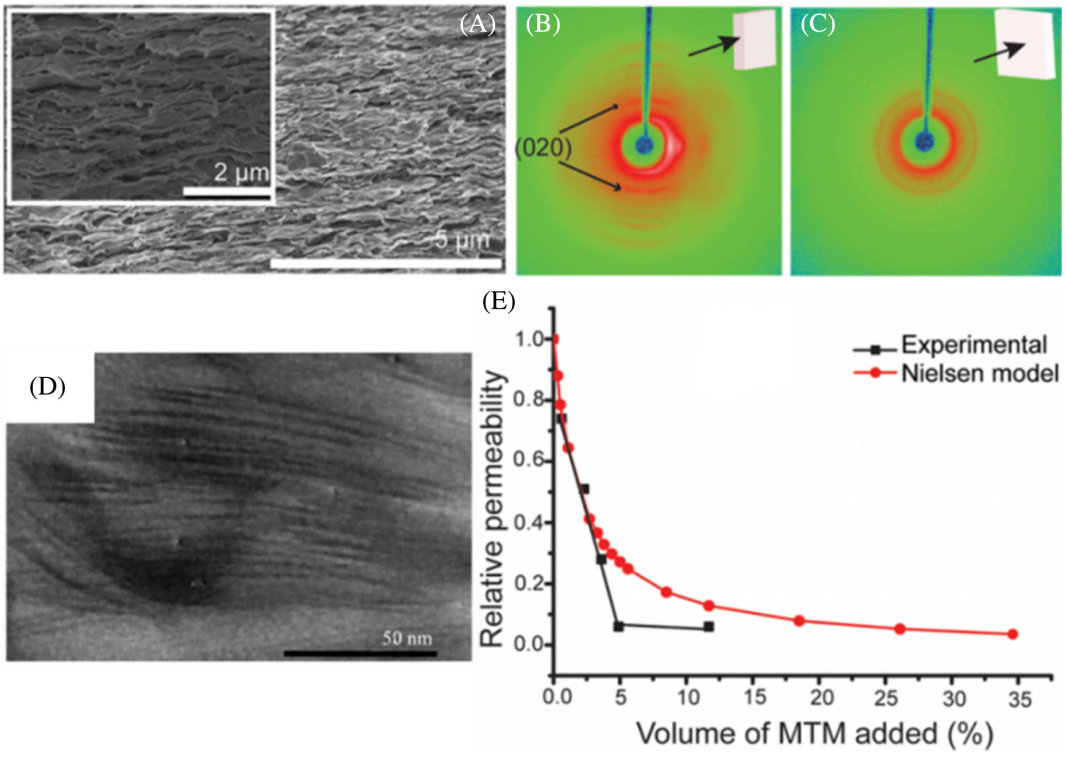

FIGURE 1 (A) SEM micrograph of a xyloglucan/clay nanocomposite at 10 wt% loading; (B) X-ray diffractogram of a xyloglucan/clay nanocomposite at 20 wt% loading in parallel and (C) perpendicular to the surface; (D) TEM micrograph of a xyloglucan/clay nanocomposite at 10 wt% loading; (E) Experimental and Nielsen model calculations for relative oxygen permeability of xyloglucan/clay nanocomposites as a function of filler (MTM) loading content. Reproduced with permission.[129] Copyright 2012, American Chemical Society

The application of solvent drying-induced alignment in preparing nanocomposites can also be extended to the biomedical field.[133–135] For example, drug release of current commercial contact lenses follows first-order kinetics, suggesting that burst release typically occurs in the initial hours, followed by several hours of low concentration release.[136–138] In order to address the challenge of slow release, Cakmak et al.[124] reported an approach to fabricate contact lenses with zero-order, constant-rate drug release. In this work, three-layer blade casting was used to prepare triple-layer films with the top and bottom layers containing vitamin E, while the middle layer was composed of antibiotic drugs. Vitamin E with anisotropic morphology was preferentially oriented (in parallel to the film surface) in both top and bottom layers. It was found that the formation of such alignment is beneficial to barrier properties. The triple layer films with oriented vitamin E demonstrated a constant-rate drug release without initial burst, which is distinct from neat vitamin E loaded single-layer films. Moreover, the triple layer film could maintain the drug concentration at a much higher level than the control sample. Therefore, the enhanced barrier property from oriented vitamin E upon solvent evaporation enables the zero-order drug delivery, which is desired for their practical applications.

Furthermore, micropatterned, high-performance soft actuators were developed based on a passive polyimide substrate containing a layer of cellulose nanofibers (CNFs), which were aligned through solvent evaporation.[139] Specifically, CNF suspension is deposited on the substrate and a static drying process follows, where capillary flow from solvent evaporation led to directional assembly of CNFs, confirmed by both SEM and polarized optical microscopy (POM). The aligned fibers exhibit anisotropic contraction and expansion, and with humidity or temperature stimuli this response can be enhanced to form a soft actuator capable of rapid bi-directional bending. The actuators displayed a fast response time (3.3 s at 40°C), excellent displacement (final curvature = 0.31 mm^{-1}), and exceptionally high lifting capacity (1000 times lifting weight ratio). Building upon these results, large-scale samples were readily prepared as well as the adaption to various metal and polymeric substrates indicating high commercialization potential. In another seminal work, large-area (up to several cm thickness and 10 cm lateral dimension) graphene/oxidized cellulose nanocrystal (OCNC) composites were fabricated with highly oriented structures upon solvent evaporation on a Teflon mold followed by thermal curing.[140] The charged OCNC surfaces facilitated the dispersion of graphene nanosheets, due to the abundance of hydrogen-bonding capable moieties effectively "gluing" to the nanosheets while crosslinking with epoxy adhesion agents. Furthermore, the OCNCs can act as a host matrix which promotes long-range alignment of graphene within the composite. This resulted in a high in-plane thermal conductivity (TC) of 25.7 W/mK, corresponding to an enhancement of 7235% through successful alignment of the embedded fillers (4.1 vol% graphene). Using a similar strategy, boron nitride nanosheets (BNNS)/ethylene-vinyl-acetate copolymer composite films with highly ordered structures can be developed through a vacuum-assisted self-assembly process, followed by drying at room temperature for 12 h.[141] The in-plane aligned BNNS enabled efficient thermally conductive pathways that allow for heat transfer, leading the composite films to exhibit an in-plane TC of 13.2 W/mK and an anisotropy ratio of 2500% at a loading content of 50 wt% BNNS. Additionally, the composite films demonstrated a retention ratio of 95% for in-plane TC after repetitive tensile tests, 98% after repetitive bending, and 97% following heating/cooling cycles, indicating mechanical flexibility and performance durability. These examples demonstrate that orienting fillers in polymer matrix through solvent evaporation is a simple and scalable method for improving composite performance in a wide variety of different applications.

2.2 | Compression molding

Compression molding is a melt processing method for fabricating polymer films (typically with over hundreds of micrometer thickness), often without the use of solvent.[142–144] In this process, a filler-containing polymer composite is heated at an elevated temperature within a mold and then compressed under high pressure, followed by cooling down to room temperature.[145–147] The high pressure applied during this compression process not only shapes/molds the polymer composite but also orients the embedded fillers with their basal plane parallel to the film surface.[148–152] For example, Liang et al.[153] found that Cloisite 15A clay nanoplatelets can be aligned in parallel to the surface of natural rubber nanocomposite films after compression molding, confirmed by XRD results. Using this method, the orientation factor of clay platelets increased with higher clay content in the rubber matrix. The high hydraulic pressure from compression molding was also employed to orient MMT clay particles in parallel to the film surface, resulting in anisotropic structures and approximately 20% decrease in the oxygen permeability of films throughout the thickness direction.[62] In another study, hot-press was utilized to fabricate oriented MMT nanoplatelets in low density polyethylene (LDPE) matrix (with only 0.5 wt% loading content), leading to approximately 7-fold

and 4-fold performance enhancement for CO_2 and O_2 barriers, respectively (compared to pure LDPE).[154] As previously described, the improved barrier properties can be attributed to the oriented nanosheets in the polymer composites, creating tortuous paths for limiting the gas molecules to diffuse and penetrate through the films.[155]

Since the compression molding process is broadly used in the polymer industry, many research efforts have leveraged its use to control the filler orientation for several advanced applications.[156–158] For example, Liu et al.[159] prepared anisotropic (3-aminopropyl) triethoxysilane (APTES)-boron nitride nanosheets (BNNS)/epoxy composites by ultrasonic exfoliation, dissolving hexagonal boron nitride powder (hBN) in a mixture of isopropanol and deionized water. Subsequently, hBN was functionalized with APTES to improve its interfacial compatibility and dispersibility in epoxy resin. The composite films were first formed by spin-coating (2000 rpm for 1 min), followed by a hot-pressing step (5 MPa at 80°C for 30 min, and fully cured at 60°C for 5 h) to align the embedded fillers. As a result, the composite exhibited excellent anisotropic TC, achieving 5.86 W/mK (in-plane direction) with a filler loading content of 40 wt%, and interfacial thermal resistance of 1.88×10^{-9} m^2K/W (an order of magnitude smaller than hBN). Hot-pressing induced hBN plate alignment in polycarbonate matrices have also been reported.[160] Specifically, a hBN/polycarbonate suspension was drop cast on a glass plate and then the film was hot-pressed at 260°C and 20 MPa for 10 min. The alignment of hBN plates from this compression process leads to the formation of thermally conductive pathways in the polymer matrix for phonon transport. The composites showed an in-plane TC of 3.09 W/mK with 18.5 vol% BN, as well as a high storage modulus of 4.26×10^9 Pa, corresponding to a respective increase of 1371% and 115.1% compared to pure polycarbonate. Additionally, a 2D thermoplastic polyurethane (TPU)/hBN elastomer composite can be prepared with up to 95 wt% hBN loading, which the filler alignment from hot-press was confirmed by SEM.[161] The resulting composite exhibited an in-plane TC of 50.3 W/mK, while the out-of-plane TC is approximately 6.9 W/mK. This high TC enabled the composite films to be efficient heat spreaders, displaying a decrease of 40°C in the saturation and set-point temperatures for light-emitting diodes.

3 | SHEAR FORCE

3.1 | Melt spinning

Melt spinning is a common technique in industry to manufacture thermoplastic polymers or polymer composite microfibers,[162–165] such as surgical and N-95 masks which have been heavily used during the COVID-19 pandemic.[166,167] To briefly introduce this process, polymer composites are first melt and pumped through a spinneret (die) containing single or multiple holes. The melt polymer fibers are then drawn, cooled, solidified, and collected on a take up wheel. Stretching of melt-spun fibers leads to the orientation of polymer chains and fillers within the composite.[168–171] The orientation factor of these filler particles is primarily controlled by the draw down ratio (DDR), which is proportional to the take-up speed of fibers.[172,173] The effect of DDR on the degree of orientation of fillers can be demonstrated by using polyamide 6/nano-clay composites as a model system.[174] At a low DDR (e.g., below 1.8), no defined X-ray scattering pattern can be observed, indicating no or very minimal orientation of nano-clay. As the DDR increased, the 2D nano-clays were oriented with their basal plane along the fiber axis and their orientation factor improved as a function of increasing DDR. In general, higher orientation factor of nano-clays in polyamide 6 leads to higher tensile strength of melt spun fibers.[174] Similarly, the melt spinning technique was used to orient one-dimensional (1D) multi-walled carbon nanotubes (MWCNTs, 2 wt% loading content) along their long axis (fibers axis) in a polycarbonate (PC) matrix.[175] The degree of alignment of MWCNTs was examined by TEM, which showed improvement with increasing DDR even though its curved shape persisted within the fibers. The composite prepared in this study can exhibit excellent stress at break (~470 MPa) with significantly higher elastic modulus (~3.25 GPa) and elongation at break (~75%) compared to PC fibers, due to the alignment of embedded MWCNTs using a DDR of 126. Furthermore, Hagstrom et al.[176] reported orienting graphite nanoplatelets (GNP) tangentially (parallel to the surface of the strand) in a polypropylene (PP) matrix by melt mixing and solid-state mixing (SSM). Compared to the melt mixed samples, the SSM samples exhibited considerably more lateral agglomeration or stacking. The in-plane aggregated GNP particles in SSM samples led to improved electrical conductivity (7.9×10^{-2} S/cm) compared to melt mixing samples (3.8×10^{-2} S/cm). The tangential orientation of GNPs also resulted in the SSM samples with glossier and smoother surfaces. Furthermore, the SSM composite displayed no plateau in storage modulus, indicating an absence of the material's yield stress, which directly corresponds to its superior spinnability. More recently, poly(methyl methacrylate) (PMMA) composites containing carbon fiber and carbon black were prepared by melt-spinning, which led to the high degree alignment of CFs along the axis of fiber composite, coupled with fence-like "conductive pathways" formed by carbon black between parallel CFs.[177]

3.2 | Film blowing

Film blowing is commonly used for producing plastic films, especially in the packaging industry,[178] where air is continuously blown into the polymer melt, resulting in its continuous expansion for film formation. As a complex, non-isothermal, and non-uniform biaxial extensional process, film blowing involves the orientation of polymer chains and fillers in the melt state, which can then be kinetically trapped upon cooling.[179,180] Through orienting filler particles in the composite films, the properties of resulting films can be improved.[178] For example, this method can be used to prepare nylon 6/clay nanocomposite films with clay layers aligned in parallel to their long axis to the film surface (Figure 2).[181] This parallel orientation enhanced the tortuosity of guest molecules for diffusion and thus reduced the permeability by more than 60% for a variety of different gases, including helium, hydrogen, water vapor, and oxygen. A systematic investigation on the effect of machine-direction DDR on the orientation of clay nanosheets in PP was also reported,[182] which showed that increasing DDRs improved the degree of orientation of the silicate layers parallel to the machine direction and thus decreasing film permeability efficiency.

In a seminal work, Nicola et al.[183] investigated the difference in the degree of orientation of graphite nanoplatelets within the LDPE matrix between compression molding and a blown extrusion process. The blown extruded samples exhibited a high degree of anisotropy in the flow direction, in comparison to the compression molded samples which were randomly oriented, leading to higher tensile strength and lower maximum strength. The Young's modulus remained similar in the transverse and machine directions, indicating the orientation may not affect polymer elasticity, only impacting the necking and recrystallization regimes. Additionally, the tensile strength increased from 15 MPa in a neat LDPE sample to 23 MPa for the oriented composite, while a higher maximum strain from 0.7 to 1.1 was achieved. Furthermore, Wang et al.[184] fabricated biodegradable poly(butylene adipate-co-terephthalate) (PBAT) containing aligned organically modified montmorillonite (OMMT) through a film-blowing process, leading to enhanced mechanical and water vapor barrier properties. As shown in Figure 3A, for

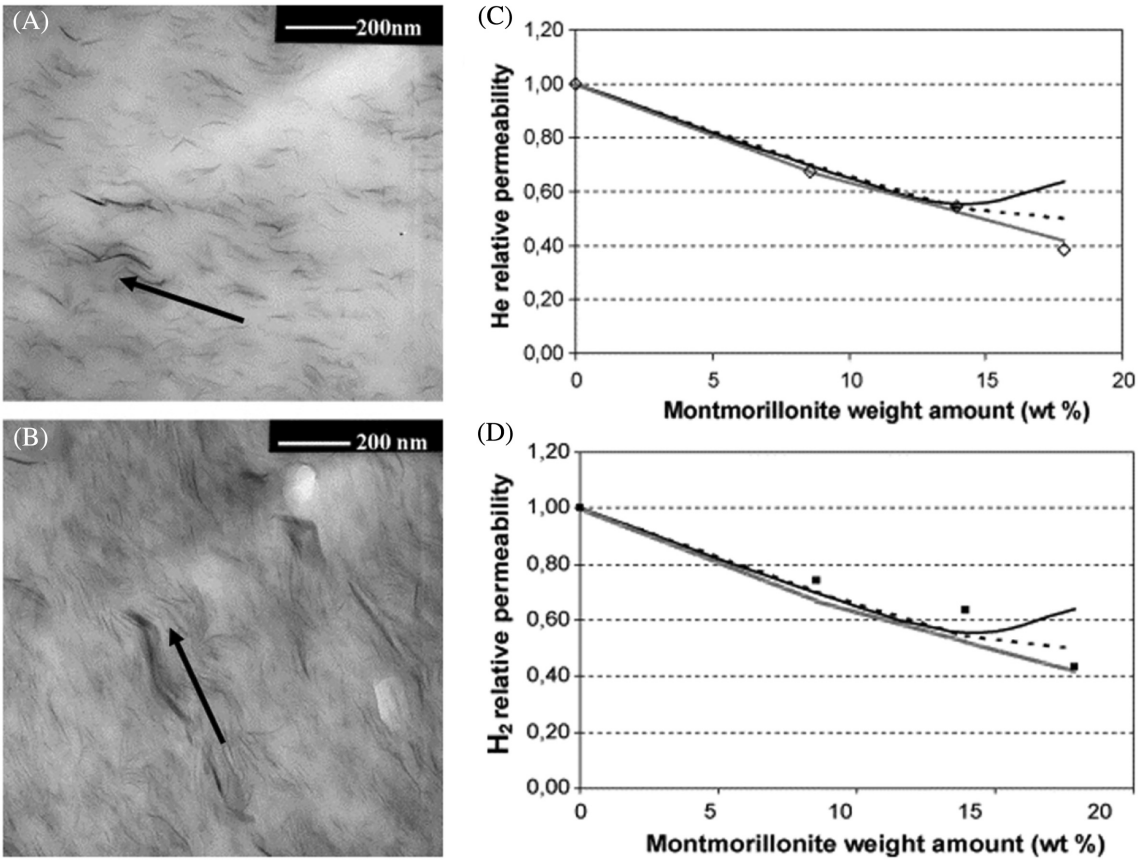

FIGURE 2 (A) TEM micrograph of nylon 6/clay nanocomposite at 6 wt% loading and (B) 13 wt% loading; (C) Theoretical permeability by Lape' model (—), Lape' model considering flake thickness polydispersity (–), Lape' model taking into account surfactant layer and flake thickness polydispersity (solid square) and experimental relative permeability for helium gas and (D) hydrogen gas. Reproduced with permission.[181] Copyright 2007, Journal of Membrane Science

films generated by the blowing process, OMMT layers can be oriented along machine direction with a small degree of tilt angle. At 13 wt% OMMT loading, the water vapor permeability decreased by 43% for the blown film compared to the pure PBAT film. However, this study found that biaxial stretching resulted in a better alignment of OMMT and further improved water vapor barrier properties (Figure 3B,C). Moreover, the Young's modulus, tensile strength at break, and elongation at break of the film blown sample at 5 wt% OMMT loading were 120 MPa, 31 MPa, and 600%, compared to 133 MPa, 69 MPa, and 185% for the biaxially oriented sample. Additionally, Manias et al. reported the alignment of MMT nano-clay in a blend of linear low-density polyethylene (LLDPE)/LDPE matrix through blown film extrusion and cold stretching.[185] The highly oriented nanofillers (in parallel to the film surface) were achieved through an industrial blown-film line with a blow-up ratio of 2, followed by annealing at 80°C for 1 week and cold stretching along the machine direction. It was found that the filler orientation could be improved with increasing shear rate. The breakdown strength of composite with 9 wt% filler loading was approximately 750 MV/m after alignment. The increased path tortuosity for charge transport in the aligned sample acted as a geometric barrier, leading to a reduced leakage current.

3.3 | Electrospinning

Electrospinning can fabricate fine polymer fibers with diameters from tens to hundreds of nanometers through the application of a static electric field.[186] The morphology of electro-spun nanofibers can be controlled by a variety of processing parameters, including voltage,[186–188] flow rate,[189,190] target distance,[191–193] solution viscosity,[194–197] and environmental humidity.[198–201] Building on the advantage of electrospinning which can improve the mechanical property through creating nanofibers with high aspect ratio,[202,203] aligning fillers within the fibers can further enhance composite performance to meet the requirement of many advanced applications. As an example, significant strengthening effects can be achieved by adding nanoparticles into the electro-spun nanofibers, especially through the inclusion of 1-D nanoparticles. In these systems, nanoparticles with a high aspect ratio can be oriented with their long axis parallel to the fiber axis,[204–207] resulting in improved mechanical, electrical, and thermal properties.[208–212] Wagner et al.[213] reported the preparation of PMMA/MWCNT composite nanofibers via electrospinning under a voltage of 6.6 kV. In this study, the morphology of MWCNTs-reinforced PMMA nanofibers from electrospinning was determined using an environmental TEM, as shown in Figure 4A. MWCNTs were completely embedded in the PMMA matrix and oriented along the fiber axis. Figure 4B shows the stress–strain curves of PMMA and PMMA/MWCNT nanofibers, and Young's modulus and tensile strength were improved by about 260% and 157%, respectively, through the inclusion of oriented MWCNTs into PMMA nanofibers.[214]

For semi-crystalline polyacrylonitrile (PAN)/MWCNT nanofiber composites prepared by electrospinning, both PAN crystals and MWCNTs can be oriented in parallel to the axis of nanofibers due to the combined effects of flow and elongation.[215] The two-dimensional XRD patterns indicated that the orientation factor for (002) plane of MWCNTs and[200] plane of PAN crystals can reach up to 0.9 and 0.62, respectively.[216] The higher orientation factor of MWCNTs than PAN polymer crystals was ascribed to the slower relaxation of MWCNTs than polymers during the drying process of nanofibers.[94,216] Compared to the pure PAN nanofiber sheets, the PAN/MWCNT sheets exhibited a 3–4 times higher tensile

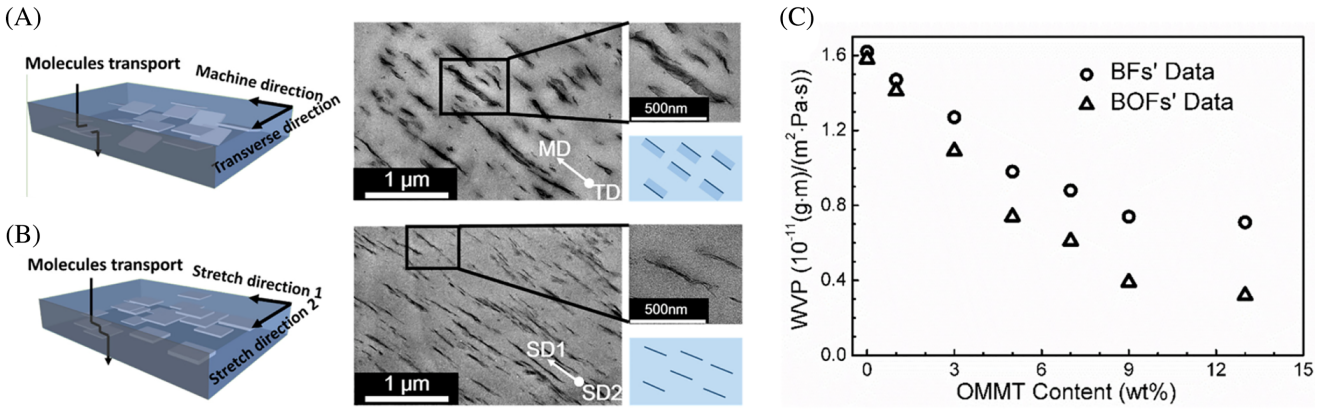

FIGURE 3 (A) Scheme and TEM micrograph of a poly(butylene adipate-co-terephthalate)-organically modified montmorillonite nanocomposite prepared by film-blowing and (B) by biaxial stretching; (C) Comparison of water vapor permeability between film blown and biaxial stretching nanocomposites at varying loading contents. Reproduced with permission.[184] Copyright 2018, American Chemical Society

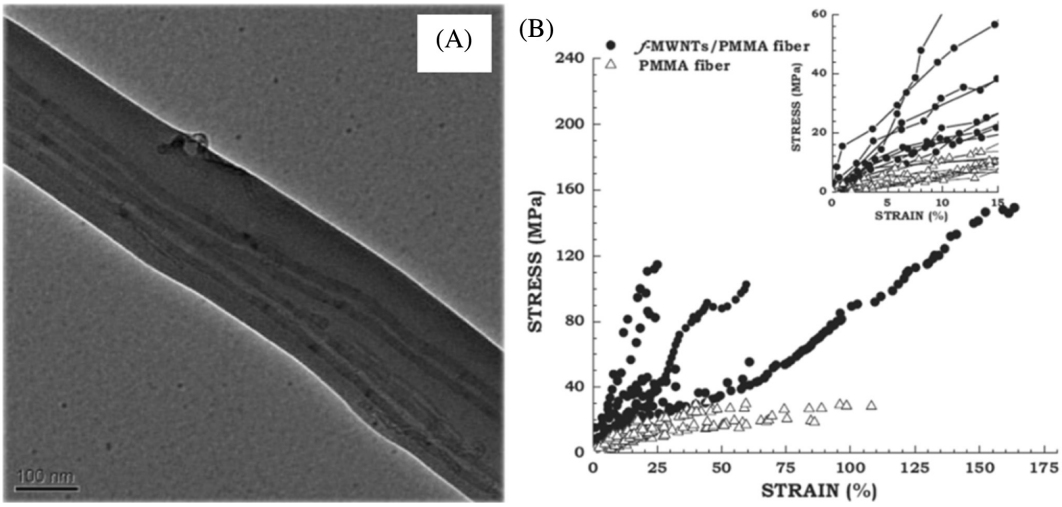

FIGURE 4 (A) TEM micrograph of CNTs in PMMA nanofiber matrix; (B) stress versus strain of neat PMMA fiber and MWCNT/PMMA fiber with an inset of the initial 15% strain range (where Young's modulus was determined through linear regression). Reproduced with permission.[213] Copyright 2007, Advanced Materials

modulus due to the presence of highly aligned MWCNT within the nanofibers. It was also demonstrated that the electrical conductivity of these PAN/MWCNT composite sheets could reach up to 0.1 S/cm, approximately two orders of magnitude higher than that of films containing randomly distributed MWCNTs.[217] Similarly, Gorga et al.[218] reported that high degree of MWCNT orientation in polyethylene oxide (PEO) nanofibers can lead to a significant improvement of electrical conductivity by almost 10^{12} as well as three times enhancement in the Young's modulus for a 1 wt% MWCNT content composite compared to pure PEO.

Electrospinning was also employed to prepare highly anisotropic, thermally conductive MWCNT/polybenzimidazole (PBI) nanofibers. Upon alignment, the in-plane TC of composite with approximately 2 wt% filler content could reach to 18 W/mK while the out-of-plane TC remained low (0.014 W/mK).[219] This was attributed to the electrospinning process which can induce highly oriented MWCNTs in PBI, creating anisotropic structures that facilitate the unidirectional phonon diffusion. Additionally, aligning fillers using electrospinning methods for improving mechanical properties of polymer composites can also be used for tissue engineering with biopolymer nanofibers. For example, Wei et al.[220] reinforced poly-(L-lactic acid) (PLLA) nanofibers with needle-shaped hydroxyapatite particles through an electrospinning process, leading to highly oriented particles along the fibral direction for enhancing mechanical properties. The particle orientation, confirmed by TEM and powder XRD, enhanced tensile strength from 17.3 to 31 MPa and elastic modulus from 388 to 1722 MPa, compared to the randomly aligned control sample.

3.4 | Post strain induced orientation of nanoparticles

The uniaxial and biaxial stretching of polymer nanocomposites can also orient embedded fillers.[221–223] For example, lead zirconate titanate (LZT) nanowires were oriented by a uniaxial stretching method along the stretching direction. The uniaxial stretching induced the orientation of nanowires, which enabled the dielectric permittivity to be 37.5% higher than a film containing randomly oriented fillers.[84] As a result, the maximum energy density enhancement through orienting nanowire improved about 51.6%. In another seminal work, poly(vinyl alcohol)/single-wall carbon nanotubes (SWCNTs) nanocomposite films were mechanically stretched to align fillers. The in-plane TC of the uniaxially stretched nanocomposite films improved with increasing draw ratios, showing a 300% increase at an optimized draw ratio of 5.5.[224] Additionally, PP/graphene nanocomposite films were stretched by sequential biaxial stretching (Figure 5A) and the graphene nanosheets were oriented in parallel to the film surface, as shown in Figure 5B.[225] In this work, in-plane electrical conductivity of 2.5 vol% graphene/PP nanocomposite film improved with increasing draw ratio, up to 4 orders of magnitude enhancement at a draw ratio of 2.4, which can be attributed to the strain induced orientation of graphene nanosheets (Figure 5C). Moreover, the anisotropy of electric resistivity (ratio of in-plane and out-of-plane resistivity) increased significantly with increased draw ratio, reaching up to 3.5×10^4 at a draw ratio of 2.4, as shown in Figure 5D.[225] Similarly, flexible, high-performance strain sensors were developed by including hybrid nanofillers (rGO with immobilized MWCNTs) in a thermoplastic

polyurethane matrix with biaxial stretching-induced alignment.[226] Nanocomposites were hot-pressed, preheated to 110 °C, and biaxially stretched at a strain rate of 10 mm/min. The aligned hybrid nanofillers improved the material stability, broadened the strain monitoring range (0.3 ∼ 400% strain), and reduced the nanocomposites resistivity (5.62 × 104 Ω m) at 2 wt% filler content in comparison to unaligned samples. Moreover, parallel alignment of the hybrid nanofillers led to enhanced sensor sensitivity (gauge factor [GF] = 150 with a 4 × 4 stretching ratio compared to a GF = 3.5 for a sensor with 30% strain). Additionally, Ding et al.[227] fabricated highly aligned silicon carbide nanowire (SiCNW)-poly(vinyl alcohol) (PVA) nanocomposites through solvent-assisted uniaxial stretching at a strain rate of 1 mm/min. Successfully orienting SiCNW enhanced the composite tensile strength by approximately 422% (188.3 MPa) and elastic modulus by 582% (6.95 GPa) compared to pure PVA. Meanwhile, the in-plane TC of the aligned nanocomposite exhibited a 105% increase (reaching 0.55 W/mK) compared to pure PVA, while maintaining a working temperature of 45.5°C.

3.5 | Flow-induced shearing

Flow-induced shearing is another simple and effective technique to align fillers in polymer composites along the shearing direction.[228–230] Graphite nanosheets can be preferentially oriented in high-density PE matrix due to the shear flow produced by a two-roll miller. The shearing induced orientation of graphite nanosheets enabled the nanocomposite to exhibit highly anisotropic conductivity with two orders of magnitude higher electrical conductivity along the in-plane than the out-of-plane direction.[231] Using a similar strategy, anisotropic nanocomposites composing of triblock copolymers and graphene particles can be prepared by flow-induced shearing.[232] Specifically, graphene nanoflakes were oriented into parallel stripes under 0.15 s^{-1} shear rate after 45 min and the aligned structure was kinetically trapped by rapid cooling of polymer matrix from 280°C to room temperature. The nanocomposite with aligned graphene stripes exhibited 2.4 × 10^4 times higher electrical conductivity than its counterpart prepared without shearing. The anisotropy factor of in-plane electrical conductivity compared to through the thickness direction is more than 1.4 × 10^4. Similarly, MWCNTs can be aligned into parallel stripes by using a similar method, with the aligned structure imparted electrical conductivity enhancement up to six orders of magnitude.[233] As another example, Tanabe et al.[234] reported the use of a doctor blade solution casting technique to orient MWCNTs in polyfurfuryl alcohol (PFA) condensate, with the cast film being cured at 160°C to trap the oriented fillers. In this work, MWCNTs were oriented along the blade casting direction due to the shearing force. The composite exhibited about a million times higher electrical conductivity than a randomly oriented film with identical MWCNT loading content. Similarly, it was found that silica and alumina particles can be aligned along the shear direction into unidirectional channels in clear polyurethane coatings,[235] accomplished by a simple drawdown method with a 75-μm gap drawdown cube with moving speeds ranging between 1 and 10 cm/s. Increasing application speed led to improved degree of alignment, confirmed by both atomic forced microscopy (AFM) and SEM techniques. Additionally, a PS/clay nanocomposite was sandwiched between two glass slides at 200 ± 10°C, and after shearing

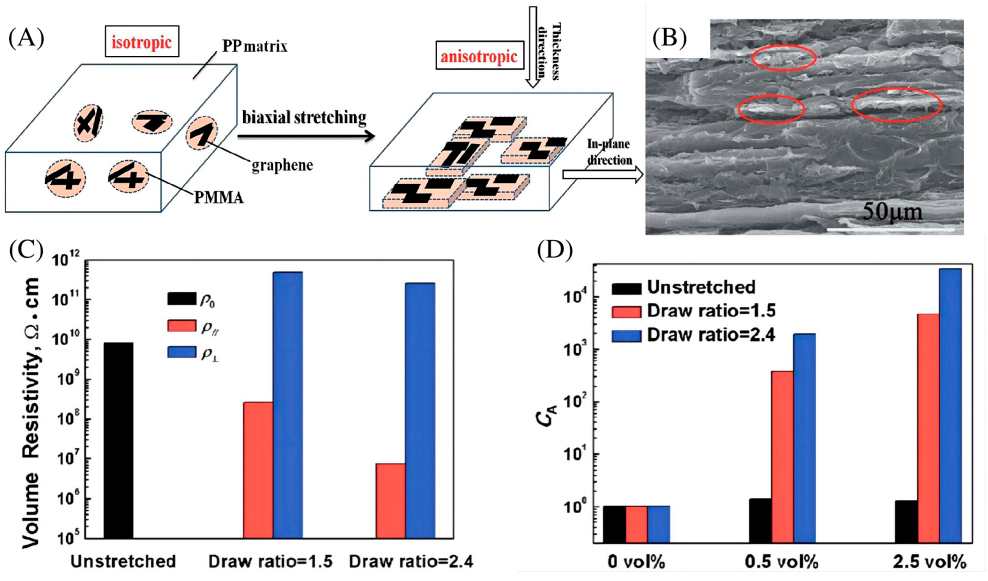

FIGURE 5 (A) Depiction of the biaxial stretching-induced alignment within PP/PMMA/graphene composites; (B) SEM micrographs displaying fracture surfaces for the nanocomposites with a draw ratio of 2.4 and a 2.5 vol% loading; (C) Volume resistivity (Ω) for nanocomposites at differing draw ratios with 2.5 vol% loading; (D) Anisotropic coefficient for nanocomposites at differing vol% loadings and draw ratios. Reproduced with permission.[225] Copyright 2017, RSC Advances

at a shear rate of 10^2 s^{-1},[236] the sharp diffraction peaks were observed from XRD, which can be attributed to the shear-induced orientation of clay particles. This result is consistent with the observation from TEM micrographs.

4 | EXTERNAL FIELDS

4.1 | Electric field

Electric field induced filler alignment in polymer composites can be accomplished using an insulating plate and two parallel electrodes.[101,237–240] Prior to applying electric field, fillers are uniformly dispersed in the polymer matrix. Subsequently, the viscous polymer solution/melt is spread and sandwiched between two electrodes. Upon the application of an external electric field, fillers are polarized and each individual particle is subjected to its neighbors' non-uniform field, leading to the formation of chain-like structures due to the attractive dielectrophoresis forces generated by dipole–dipole interactions.[241] 1D and 2D particles can be rotated under such force with their long axis along the electric field direction, forming chains with head-to-tail structures. In most cases, the aligned structure of particle chains in the polymer matrix can be gradually relaxed back to a randomly distributed state after removal of the electric field. Therefore, this method is often coupled with solidification of polymer composites by solvent evaporation, crosslinking the matrix, or quenching the melts prior to removing the electric field in order to kinetically trap the aligned structure.

Electric-field induced filler alignment often improves electrical and thermal conductivity of polymer composites. For example, in-plane alignment of SWCNTs in a photo-curable matrix (urethane dimethacrylate (UDMA) and 1,6-hexanediol dimethacrylate (HDDMA) blend) results in the electrical conductivity increasing from 3.3×10^{-13} S/cm to 10^{-7} S/cm, approximately six orders of magnitude enhancement as reported by Harrison et al.[242] In this study, the alignment was achieved by alternating current (AC) field-induced dipolar interactions between SWCNTs within a liquid media, followed by a step of photopolymerization while under a constant electric field. Bauhofer et al.[243] found that upon electric field-induced alignment, a carbon nanofiber/epoxy resin composite exhibited a dielectric constant that is 30 times higher than control samples containing randomlyoriented carbon nanofibers. Additionally, Robertson et al.[244] investigated the effect of electric field-induced orientation of short glass fibers on the toughening behaviors of UDMA/HDDMA composites. As the fracture surface was perpendicular to the axis of aligned glass fibers, the composites with aligned fibers displayed an increase of 40%, 50%, and 145% in fracture toughness, flexural modulus, and fracture energy, respectively, compared to the composites with randomly oriented fibers.[244]

The application of external fields often results in out-of-plane alignment of nanoparticles, which is difficult to observe directly using an optical microscope. To address this challenge, Cakmak et al.[245] reported the orientation kinetics of clay platelets by measuring the real-time change in birefringence of clay/photocurable resin composites, as shown in Figure 6A. The anisotropic optical refractive index of clay resulted in the development of birefringence after the application of electric field.[246] To briefly describe this alignment process, the torque induced by dielectrophoresis initially rotated the clay platelets with their basal plane parallel the electric field. Subsequently, the rotated clay platelets were aligned into chain structures due to dipole–dipole interactions. As a result, birefringence increased slowly and reached a plateau under lower voltages, while at higher voltages birefringence increased rapidly to a higher plateau value. The cross-sectional morphology of the photocured nanocomposite films shown in Figure 6B displays the vertical alignment of clay particles across the entire sample. The XRD patterns of clay crystals ([001] plane) (Figure 6C) were transformed from a circle into arcs, indicating the successful orientation of clay platelets along the thickness direction. In Figure 6D, the nanocomposite films with aligned clay platelets exhibited higher dielectric permittivity when frequency is below 0.03 Hz, which is attributed to the enhancement of through-thickness ionic conductivity.[247,248]

Additionally, electric field assisted assembly of barium strontium titanate (BST) in a thermally curable PU showed that nanocomposite films with aligned fillers exhibit three times higher dielectric permittivity than a film with randomly oriented particles, when filler content is 22 vol%.[249] Similarly, the electric field-induced alignment of barium titanate ($BaTiO_3$) in thermally curable poly(dimethylsiloxane) (PDMS) improved dielectric permittivity by at least 50% as opposed to the control samples (i.e., no orientation of fillers) at the same filler loading content. While the electric field induced alignment of nanoparticles in thermal or photo curable matrix has been relatively well developed, their assembly in thermoplastic polymer/solvent solutions may have additional processing challenges, which are associated with structural relaxation in the matrix. To address this issue, a novel processing method was developed to achieve "Z" direction alignment of nanoparticles in polymer/solvent solutions for preparing nanocomposites with enhanced through-thickness dielectric properties.[250] As shown in Figure 7A, the alignment kinetics of $BaTiO_3$ were studied

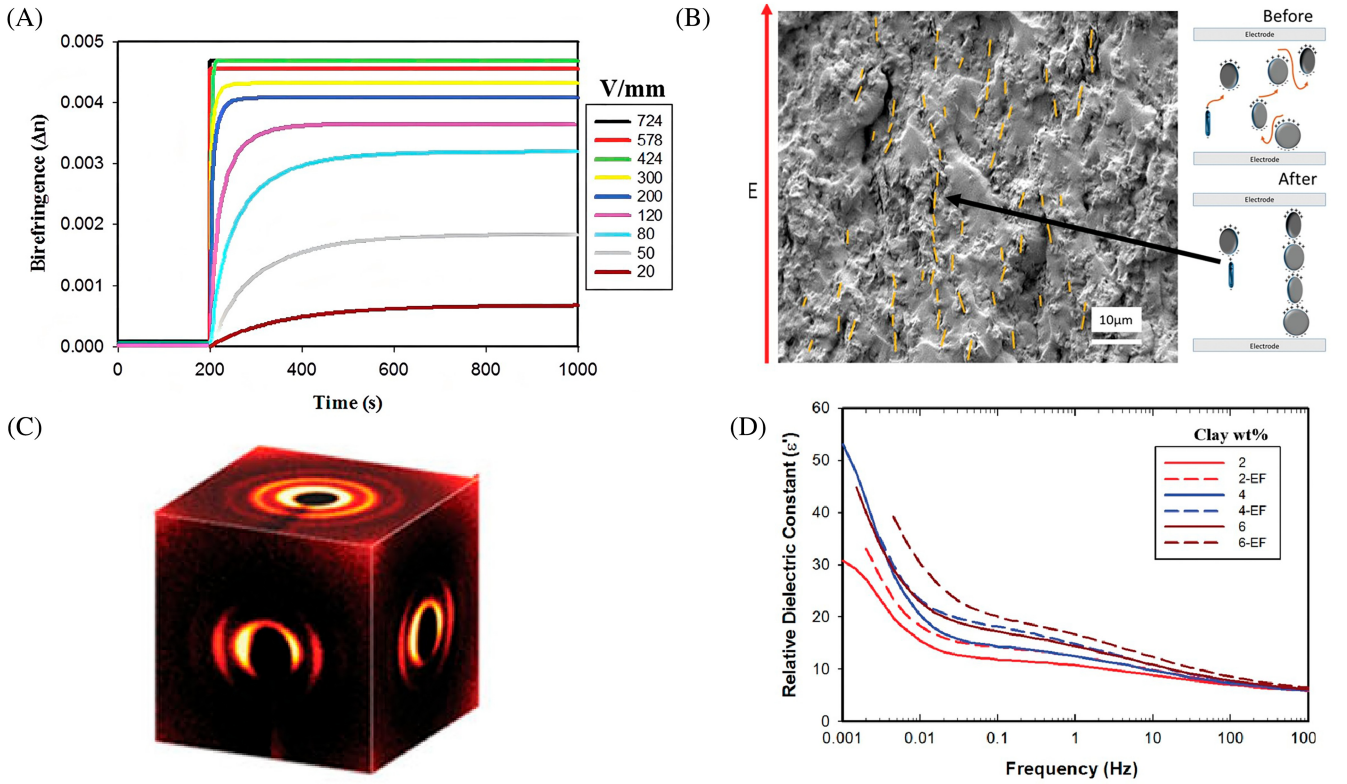

FIGURE 6 (A) Clay alignment kinetics displayed through birefringence versus time for nanocomposites with 2 wt% loading at various voltages; (B) SEM micrograph displaying clay platelet chaining with highlighted platelet edges and a dielectrophoretic chaining diagram; (C) XRD patterns for the nanocomposite in three principal directions; (D) Relative dielectric constant enhancement with increasing nanocomposite clay loading. Reproduced with permission.[245] Copyright 2014, Advanced Functional Materials

by measuring the real-time change in light transmission of wet films, demonstrating the competition between solvent evaporation-induced shrinkage force and dielectrophoresis force on structures. Once the electric field is applied, the dielectrophoresis force induced the alignment of short $BaTiO_3$ chains. This led to a rapid increase in light transmission, which further increased, though at a slower rate due to the growth of chains of particles. As more solvent evaporated, the light transmission decreased since this resulted in internal film stresses, which can potentially buckle the aligned particle chains. As shown in Figure 7B, the aligned nanoparticle chains were tilted to an angle between the chain axis and the electric field direction (instead of perfectly along the field direction). This angle became smaller, and the light transmission increased to higher values when applying a stronger electric field, suggesting the formation of more vertically aligned nanoparticles. In this study, the critical electric field strength to achieve vertical alignment was approximately 1500 V/mm. The resulting nanocomposite films exhibited increased dielectric permittivity improvement when vertical alignment of $BaTiO_3$ chains was enhanced by increasing field strength, as shown in Figure 7C.

Moreover, Helgesen et al.[251] found that the alignment of carbon nano-cones within a commercial two component epoxy-amine adhesive resulted in 2–3 orders of magnitude higher electrical conductivity, even at a very low loading content of 0.2 vol%. Wang et al.,[47] studied the effect of electric field assisted alignment of multilayer graphene on the electrical and thermal conductivity of epoxy nanocomposites. The nanocomposites with aligned graphene plates exhibited 2–3 orders of magnitude enhancement and an approximately 60% increase in the electrical and thermal conductivity, respectively, compared to films with randomly oriented graphene at the same loading level. Similarly, a 145% improvement in the TC of PDMS/diamond nanocomposites was reported through aligning 5 vol% diamond particles using an electric field.[252] The electric field assisted assembly of nanoparticles was demonstrated to be compatible with roll-to-roll continuous processing to enable large-scale manufacturing of high performance nanocomposites with aligned fillers, such as preparing PDMS nanocomposites with "Z" oriented graphite nanoplatelets.[253] In this study, an increase of 25,000% and 150% was observed in electrical and thermal conductivities of nanocomposites, respectively, by aligning 5 vol% graphite. Moreover, such alignment resulted in the

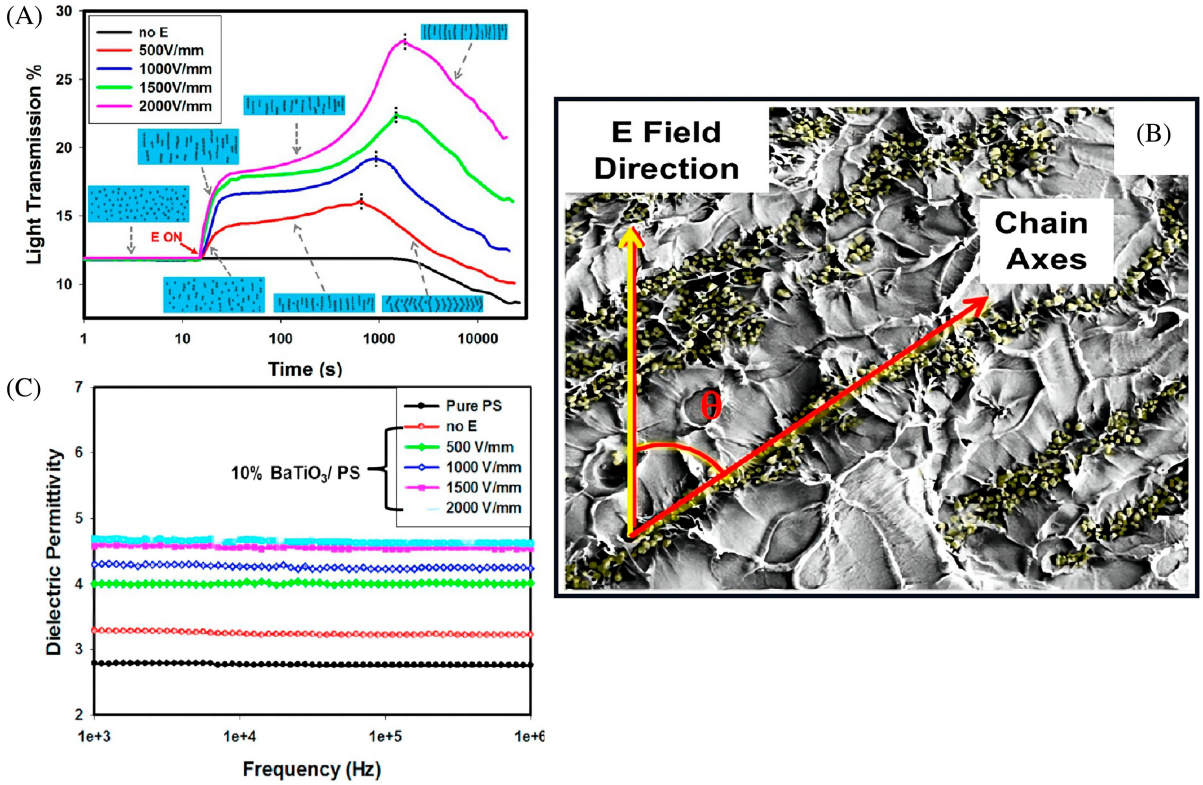

FIGURE 7 (A) Light transmission as a function of time throughout the solution drying process for various initial electric field strengths; (B) SEM micrograph of the nanocomposite prepared with an electric field of 1000 V/mm (scale bar: 40 μm); (C) Initial electric field effect on dielectric permittivity. Reproduced with permission.[250] Copyright 2016, American Chemical Society

percolation threshold concentration for the optimized electrical conductivity decreasing substantially from 10 to 2 vol %. Similarly, Chen et al.[254] reported that nickel coated PS microspheres can be aligned in the epoxy matrix, resulting in the conductivity of aligned composites which was approximately three orders of magnitude higher than the unaligned composite ($\sim 10^{-5}$ to $\sim 10^{-2}$ S/m) at a loading content of 15 wt%.

More recently, Zhang et al.[255] reported that silver-coated fibrotic cellulose (SFCs) can be aligned in PDMS matrix along the out-of-plane direction ("Z") through the use of an electric field in order to enhance dielectric permittivity and anisotropic light transmission. After alignment, the dielectric constant of SFCs/PDMS composites was increased by a factor of 3.5, while the increase of dielectric loss was fairly minimal (<2.1%). The alignment of cellulose in the flexible polymer matrix could be utilized in the manufacturing of wearable electronics. Subsequently, another work showed that ternary composites with high dielectric permittivity and low dielectric loss can be fabricated by creating barriers in the aligned conductive channels.[256] Specifically, as shown in Figure 8A, the particle chains formed by graphite can significantly improve the dielectric permissibility in the flexible polymer matrix (e.g., PDMS) under an electric field. Meanwhile, the insulating particles ($BaTiO_3$) are embedded in the potential conductive chain as a barrier, which can inhibit leakage current and produce low dielectric loss. Figure 8B demonstrated that by aligning 2.5 wt% graphite particles and 5 wt% $BaTiO_3$ through electric field, the ternary composite can exhibit a significantly improved dielectric constant as high as 73 and a dielectric loss as low as 0.19.

4.2 | Magnetic field

Similar to the electric field, magnetic field can also be employed to fabricate polymer composites with anisotropic structures and enhanced properties, through assembly of both ferromagnetic particles (nickel,[257,258] iron[259] and cobalt[260] etc.) and/or non-ferromagnetic systems, including molecular chains,[261,262] phase-separated domains,[262,263] and diamagnetic particles.[264,265] Compared to ferromagnetic particles, the strength of magnetic field required to orient non-ferromagnetic fillers is much higher due to their lower susceptibility. Here, we focus on discussing the magnetic field induced orientation and assembly of ferromagnetic materials. The magnetic field induces the formation of

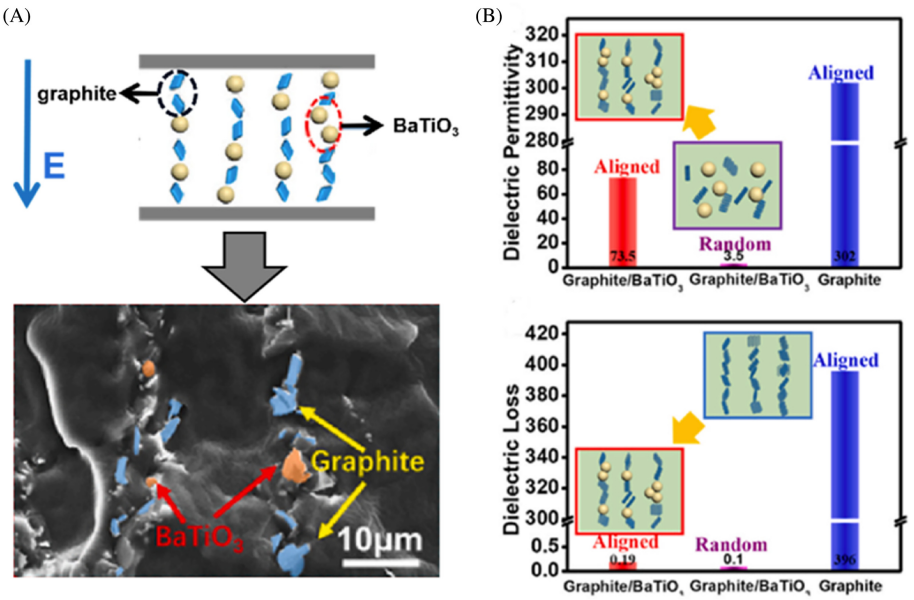

FIGURE 8 (A) Schematic illustration and SEM micrograph of the mechanism of $BaTiO_3$ particles and graphite chain forming under an electric field; (B) Dielectric permittivity and dielectric loss at 10^2 Hz of aligned and randomly oriented nanocomposites, and aligned graphite with graphite loading of 2.5 wt% and barium titanate loading of 5 wt%. Reproduced with permission.[256] Copyright 2021, Composites Science and Technology

magnetic dipoles within these particles,[266,267] which is similar to the electric field in principle. The polarized ferromagnetic particles are self-assembled into chain like structures due to dipole–dipole attractions, lowering the magnetostatic energy in the field direction.

Compared with the electric field, the magnetic field has better conduction performance because it does not require direct contact between the magnetic pole and the sample, which brings great convenience in the practical manufacturing process.[268,269] In general, ferromagnetic substances, such as iron, cobalt, and nickel, can be magnetized very easily under low magnetic fields (even mT is enough), while diamagnetic substances usually require over 5 T magnetic fields for enabling successful alignment. The alignment of ferromagnetic Fe_2O_3 nanorods with core-shell structures can be achieved in PEO-lithium perchlorate ($LiClO_4$) based electrolytes through a simple neodymium magnetic device.[270] Samples were cast from solution while exposed to a 0.5 T magnetic field. This method led to the alignment of nanorods perpendicular to the electrode, confirmed by SEM micrographs. The polymeric electrolytes with magnetically aligned nanorod samples can eliminate structural disorder with improved homogeneity, performance consistency, and degree of crystallinity in the PEO/$LiClO_4$. In a seminal work, Dean et al.[271] oriented diamagnetic SWCNTs in a polyethylene terephthalate (PET) matrix through a magnetic resonance imaging (MRI) scanner with a 3 T or a 9.4 T magnetic field and investigated their electrical properties as a function of the degree of alignment. It was found that the alignment can be improved with a higher magnetic field strength and a lower filler concentration. When compared to a sample without magnetic field exposure, the aligned nanocomposite with 3 wt% SWCNT showed significant electrical behavior changes at low frequencies. Specifically, the increase in non-dielectric range and electrical conductivity suggests the magnetic field exposure facilitates the dispersion, which led to the improved electron "hopping" by minimizing gaps between particles. It was further determined that at 0.5 wt% SWCNT loading, the aligned nanocomposite exhibited sufficient electrical conductivity for antistatic and electrostatic dissipation. Furthermore, superparamagnetic particles can also be aligned under the application of magnetic fields, which Billaud et al. reported a simple and effective method to enhance the magnetic response of diamagnetic graphite.[272] Specifically, using a simple rotating magnetic field, they successfully aligned graphite sheets in poly(vinyl pyrrolidone) (PVP) (Figure 9), resulting in an increase of their electrode's lithium storage capacity by a factor of 3. The oriented graphite sheets led to facilitated transport pathways for conducting lithium ions. According to the calculation, the tortuosity of the conducting path after the orientation was almost four times lower than their counterparts without orienting the fillers.

Furthermore, Chen et al.[273] reported the alignment of ferric oxide (Fe_3O_4) nanoparticles/tunicate cellulose nanocrystal (t-CN) hybrids in epoxidized natural rubber by employing a low magnetic field. In this work, the optimal magnetic field intensity was found to be 0.2 T for the alignment of t-CN/Fe_3O_4 hybrids, which can result in a storage modulus of 2384 MPa and a tensile strength of 3.6 MPa for a parallelly aligned sample; both are much higher than a randomly oriented sample at 5 phr. The magnetization of the composites was also enhanced

through filler alignment and can be further improved with increasing the loading content of t-CN/Fe_3O_4 hybrids, achieving 3.24 emu/g at 5 phr. The alignment of magnetic composite nanofluid fillers (MWCNTs and graphene oxides in a polyether shell) in an epoxy matrix was also demonstrated.[274] The directional alignment of embedded nanoparticles (with 1 wt% filler content), promoted by a magnet on both sides with varied magnetic field strength (0.3 and 0.6 T), enhanced the impact strength of the composite by 136.5% (reaching 60.3 kJ/m^2) and the bending strength by 30.9% (reaching 113.2 kJ/m^2) compared to the neat epoxy. Moreover, Mazinani et al.[275] found improved mechanical properties by aligning Fe_3O_4 in PVA nanocomposites through the application of a very low magnetic field (750 G). The samples exposed to the magnetic field displayed higher crystallinity where at 0.1 wt% Fe_3O_4, crystallinity was increased by 57% compared to the pure PVA and 81% compared to a randomly oriented sample. Similarly, the toughness, modulus, tensile strength, and elongation at break were increased by 55%, 67%, 143%, and 37%, respectively, at 0.1 wt% loading content compared to randomly oriented samples. Furthermore, TC of hybrid nanoparticles (magnetic needle-like ferro oxide and reduced graphene oxide) in a boron nitride/polyimide composite can also be improved through alignment upon using a moving magnetic field.[276] It was found that at 30 wt% loading, its in-plane TC was improved by 1233% (2.532 W/mK) and the out-of-plane TC was improved by 150% (0.425 W/mK) compared to the pure polyimide. Furthermore, the aligned composite also showed improved flexibility, dielectric properties, and tensile properties compared to the neat polymer. Similarly, magnetic bentonite nanoparticles can be aligned in LDPE matrix by applying a 1 T magnetic field using a commercial Nd-Fe-B ring magnet.[277] In this study, nanoparticle alignment was confirmed by optical microscopy (OM) and atomic force microscopy (AFM), which also led to improved dispersion and degree of crystallinity compared to the non-aligned samples. As a result, the storage modulus of the aligned samples was enhanced by 43% compared to the pure polymer and 18% compared to the pure clay.

5 | CONCLUDING REMARKS AND FUTURE PERSPECTIVES

In summary, directional assembly of fillers within polymer composites can improve material properties, enhancing their use for a variety of applications. For example, in-parallel alignment of 2D fillers can improve the gas barrier properties of composites by creating more tortuous diffusion paths. While various methods have been developed toward this goal, industrially relevant approaches still often rely on the use of compression force, shear force, or external fields, as these methods are compatible with current manufacturing processes and are relatively easy to scale up. Compression force can be introduced through molding processes or solution evaporation to effectively orient fillers in parallel to the film surface. Shear force leads to the orientation of polymer chains and fillers inside polymer composites which improves mechanical, electrical, and thermal properties. Shear field can be introduced during melt spinning, film blowing, electrospinning, and solution

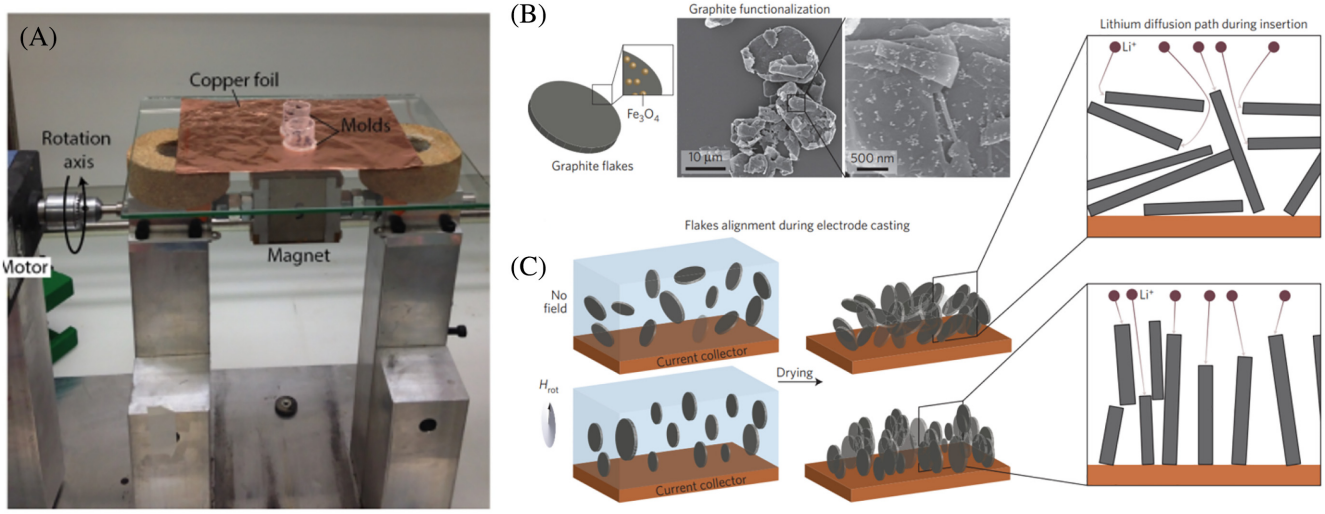

FIGURE 9 (A) Apparatus for preparation of graphite-PVP nanocomposite under magnetic field; (B) Diagram and SEM micrograph of ferric oxide-coated graphite flakes; (C) Graphite flake alignment and lithium diffusion pathway under no magnetic field (top) and under a rotating magnetic field. Reproduced with permission.[272] Copyright 2016, Nature Energy

casting. Applying external fields (both electric and magnetic) can assist the directional assembly of different particles within the polymer matrix along the field direction, often throughout the film thickness. Furthermore, recent reports indicate that external fields can be implemented into the roll-to-roll processing line, allowing their use in large-scale manufacturing.[278–280] This approach could potentially provide a commercially viable platform for the continuous production of polymer composites embedded with aligned fillers.

Moving forward, additive manufacturing (AM) processes are now becoming an emerging technology with enormous potential for mass production and rapid prototyping.[281–287] AM has several distinct advantages over conventional manufacturing methods, including design flexibility,[288–291] and significant reduction in overall processing time,[292,293] energy consumption,[294–296] and waste generation,[297–299] making it very compelling for the polymer industry. Over the past decade, intensive research efforts have been focused on improving printing resolution,[300,301] accelerating printing rate,[302,303] and enabling the precise structural control across multiple length scales.[304–307] However, the ability to prepare polymer composites with aligned fillers is much less developed.[308] Therefore, significant opportunities exist for combining some of these established methods in AM through leveraging different external forces and fields, ultimately toward creating anisotropic and performance-enhanced polymer composites with versatile control over material shape, size, and functionality.

ACKNOWLEDGMENTS

Anthony Griffin and Zhe Qiang would like to acknowledge National Science Foundation Office of Integrative Activities #1757220 for the support.

ORCID

Yuwei Chen https://orcid.org/0000-0001-6955-4704
Zhe Qiang https://orcid.org/0000-0002-3539-9053

REFERENCES

[1] H. Jariwala, P. Jain, V. Maisuriya, *Polym. Compos.* **2021**, *42*(3), 1407.
[2] S. M. Zachariah, Y. Grohens, N. Kalarikkal, S. Thomas, *Polym. Compos.* **2022**, *43*(5), 2507.
[3] S. Gaheen, G. W. Hinkal, S. A. Morris, C. Khoa Nguyen, N. Quyen Tran, T. Phuong Nguyen, D. Hai Nguyen, *Adv. Nat. Sci. Nanosci. Nanotechnol.* **2017**, *8*(1), 015001.
[4] P. Allia, G. Barrera, P. Tiberto, T. Nardi, Y. Leterrier, M. Sangermano, *J. Appl. Phys.* **2014**, *116*(11), 113903.
[5] Z. Chen, B. Mai, H. Tan, X. Chen, *Compos. Commun.* **2018**, *10*, 194.
[6] W. Jian, D. Hui, D. Lau, *Nanotechnol. Rev.* **2020**, *9*(1), 700.
[7] J. Njuguna, K. Pielichowski, J. Fan, *Adv. Polym. Nanocompos. Types Appl.* **2012**, *15*, 472.
[8] J. Njuguna, K. Pielichowski, *Adv. Eng. Mater.* **2003**, *5*(11), 769.
[9] A. Bhat, S. Budholiya, S. A. Raj, M. T. H. Sultan, D. Hui, A. U. M. Shah, S. N. A. Safri, *Nanotechnol. Rev.* **2021**, *10*(1), 237.
[10] E. J. Siochi, J. S. Harrison, *MRS Bull.* **2015**, *40*(10), 829.
[11] K. Ramachandran, V. Boopalan, J. C. Bear, R. Subramani, *J. Mater. Sci.* **2022**, *57*(6), 3923.
[12] G. Balaganesan, N. K. Gupta, R. Velmurugan, *Adv. Compos. Aerosp. Eng. Appl.* **2022**, *2*, 23.
[13] S. Chen, A. Skordos, V. K. Thakur, *Mater. Today Chem.* **2020**, *17*, 100304.
[14] X. Huang, B. Sun, Y. Zhu, S. Li, P. Jiang, *Prog. Mater. Sci.* **2019**, *100*, 187.
[15] Q. Wang, L. Zhu, *J. Polym. Sci. Part B Polym. Phys.* **2011**, *49*(20), 1421.
[16] L. Ji, P. Meduri, V. Agubra, X. Xiao, M. Alcoutlabi, L. Ji, X. Xiao, P. Meduri, V. Agubra, M. Alcoutlabi, *Adv. Energy Mater.* **2016**, *6*(16), 1502159.
[17] C. Yang, H. Wei, L. Guan, J. Guo, Y. Wang, X. Yan, X. Zhang, S. Wei, Z. Guo, *J. Mater. Chem. A* **2015**, *3*(29), 14929.
[18] H. Kumar, R. Sharma, A. Yadav, R. Kumari, *J. Energy Storage* **2021**, *33*, 102032.
[19] V. B. Yadav, R. Gadi, S. Kalra, *J. Environ. Manage.* **2019**, *232*, 803.
[20] T. A. Saleh, P. Parthasarathy, M. Irfan, *Trends Environ. Anal. Chem.* **2019**, *24*, e00067.
[21] Mukhopadhyay, R.; Bhaduri, D.; Sarkar, B.; Rusmin, R.; Hou, D.; Khanam, R.; Sarkar, S.; Kumar Biswas, J.; Vithanage, M.; Bhatnagar, A.; Ok, Y. S., *J. Hazard. Mater.* **2020**, *383*, 121125.
[22] E. I. Unuabonah, A. Taubert, *Appl. Clay Sci.* **2014**, *99*, 83.
[23] N. Pandey, S. K. Shukla, N. B. Singh, *Nanocomposites* **2017**, *3*, 47.
[24] C. I. Idumah, A. Hassan, D. E. Ihuoma, *Polym.-Plast. Technol. Mater.* **2019**, *3*, 1054.
[25] U. Qasim, A. I. Osman, A. H. Al-Muhtaseb, C. Farrell, M. Al-Abri, M. Ali, D. V. N. Vo, F. Jamil, D. W. Rooney, *Environ. Chem. Lett.* **2020**, *19*(1), 613.
[26] J. Wróblewska-Krepsztul, T. Rydzkowski, G. Borowski, M. Szczypiński, T. Klepka, V. K. Thakur, *Int. J. Polym. Anal. Charact.* **2018**, *23*(4), 383.
[27] J. Sarfraz, T. Gulin-Sarfraz, J. Nilsen-Nygaard, M. K. Pettersen, *Nanomater* **2021**, *11*, 10.
[28] S. Veprek, M. J. G. Veprek-Heijman, *Surf. Coat. Technol.* **2008**, *202*(21), 5063.
[29] E. Yarahmadi, K. Didehban, M. G. Sari, M. R. Saeb, M. Shabanian, F. Aryanasab, P. Zarrintaj, S. M. R. Paran, M. Mozafari, M. Rallini, D. Puglia, *Prog. Org. Coat.* **2018**, *119*, 194.
[30] N. H. Othman, M. Che Ismail, M. Mustapha, N. Sallih, K. E. Kee, R. Ahmad Jaal, *Prog. Org. Coat.* **2019**, *135*, 82.
[31] T. Sainsbury, S. Gnaniah, S. J. Spencer, S. Mignuzzi, N. A. Belsey, K. R. Paton, A. Satti, *Carbon* **2017**, *114*, 367.
[32] O. Chaabouni, S. Boufi, *Carbohydr. Polym.* **2017**, *156*, 64.
[33] H. Kang, Y. Tang, L. Yao, F. Yang, Q. Fang, D. Hui, *Compos. Part B Eng.* **2017**, *112*, 1.
[34] Y. Guo, J. Drum, C. Qu, M. Cakmak, *Polym. Compos.* **2016**, *37*(3), 709.

[35] J. P. Cao, X. Zhao, J. Zhao, J. W. Zha, G. H. Hu, Z. M. Dang, *ACS Appl. Mater. Interfaces* **2013**, *5*(15), 6915.
[36] H. Guo, X. Li, B. Li, J. Wang, S. Wang, *Mater. Des.* **2017**, *114*, 355.
[37] M. Sureshkumar, H. Y. Na, K. H. Ahn, S. J. Lee, *ACS Appl. Mater. Interfaces* **2015**, *7*(1), 756.
[38] S. Jafarzadeh, P. M. Claesson, P. E. Sundell, J. Pan, E. Thormann, *ACS Appl. Mater. Interfaces* **2014**, *6*(21), 19168.
[39] S. Mondal, S. Ganguly, P. Das, D. Khastgir, N. C. Das, *Compos. Part B Eng.* **2017**, *119*, 41.
[40] S. Wang, Y. Jing, *Appl. Clay Sci.* **2017**, *138*, 74.
[41] H. Kim, H. N. Ra, M. Kim, H. G. Kim, S. S. Kim, *Prog. Org. Coat.* **2017**, *108*, 25.
[42] T. T. Santos, T. G. Almeida, D. D. S. Morais, F. D. Magalhães, R. M. Guedes, E. L. Canedo, L. H. Carvalho, *Polym. Bull.* **2019**, *77*(2), 901.
[43] G. Z. Papageorgiou, D. S. Achilias, S. Nanaki, T. Beslikas, D. Bikiaris, *Thermochim. Acta* **2010**, *511*(1–2), 129.
[44] C. Harito, D. V. Bavykin, B. Yuliarto, H. K. Dipojono, F. C. Walsh, *Nanoscale* **2019**, *11*(11), 4653.
[45] C. O. Blattmann, S. E. Pratsinis, *Kona Powder Part. J.* **2019**, *36*, 2019015.
[46] Z. M. Dang, H. Y. Wang, Y. H. Zhang, J. Q. Qi, *Macromol. Rapid Commun.* **2005**, *26*(14), 1185.
[47] S. Wu, R. B. Ladani, J. Zhang, E. Bafekrpour, K. Ghorbani, A. P. Mouritz, A. J. Kinloch, C. H. Wang, *Carbon* **2015**, *94*, 607.
[48] W. Benhadjala, M. Gravoueille, I. Bord-Majek, L. Béchou, E. Suhir, M. Buet, M. Louarn, M. Weiss, F. Rougé, V. Gaud, Y. Ousten, *Appl. Phys. Lett.* **2015**, *107*(21), 211903.
[49] F. Ebrahimi, A. Seyfi, *Mech. Based Des. Struct. Mach.* **2019**, *49*(1), 59.
[50] A. H. Esbati, S. Irani, *Mech. Mater.* **2018**, *118*, 106.
[51] X. Li, W. Park, Y. P. Chen, X. Ruan, *J. Heat Transfer* **2017**, *139*(2), 022401.
[52] L. Lisuzzo, G. Cavallaro, S. Milioto, G. Lazzara, *Appl. Clay Sci.* **2020**, *185*, 105416.
[53] A. Wagih, A. Abu-Oqail, A. Fathy, *Ceram. Int.* **2019**, *45*(1), 1115.
[54] A. Sharma, T. Mandal, S. Goswami, *Nano-Struct. Nano-Objects* **2021**, *25*, 100642.
[55] C. Park, Z. Ounaies, K. A. Watson, R. E. Crooks, J. Smith, S. E. Lowther, J. W. Connell, E. J. Siochi, J. S. Harrison, T. L. St Clair, *Chem. Phys. Lett.* **2002**, *364*(3–4), 303.
[56] X. Na, J. Qingjie, Z. Chongguang, W. Chenglong, L. Yuanyuan, *Mater. Des.* **2010**, *31*(4), 1676.
[57] T. D. Ngo, M. T. Ton-That, S. V. Hoa, K. C. Cole, *Compos. Sci. Technol.* **2009**, *69*(11–12), 1831.
[58] M. Ashjari, A. R. Mahdavian, N. G. Ebrahimi, Y. Mosleh, *J. Inorg. Organomet. Polym. Mater.* **2010**, *20*(2), 213.
[59] Y. Fu, P. Zheng, Y. J. Qiu, J. Liu, Y. L. Zhang, L. Lu, H. Guo, *Polym. Compos.* **2022**, *43*(5), 2651.
[60] K. Wakabayashi, C. Pierre, D. A. Diking, R. S. Ruoff, T. Ramanathan, L. Catherine Brinson, J. M. Torkelson, *Macromolecules* **2008**, *41*(6), 1905.
[61] K. Wang, S. Liang, R. Du, Q. Zhang, Q. Fu, *Polymer (Guildf)* **2004**, *45*(23), 7953.
[62] S. Shafiei Sabet, A. A. Katbab, *J. Appl. Polym. Sci.* **2009**, *111*(4), 1954.
[63] M. Felisberto, A. Arias-Durán, J. A. Ramos, I. Mondragon, R. Candal, S. Goyanes, G. H. Rubiolo, *Phys. B* **2012**, *407*(16), 3181.
[64] L. S. Su, J. L. Tsai, *Polym. Compos.* **2021**, *42*(8), 4005.
[65] S. Ghaffari-Mosanenzadeh, O. Aghababaei Tafreshi, E. Dammen-Brower, E. Rad, M. Meysami, H. E. Naguib, *Polym. Compos.* **2022**, *43*(2), 692.
[66] A. A. Hassen, R. B. Dinwiddie, S. Kim, H. L. Tekinap, V. Kumar, J. Lindahl, P. Yeole, C. Duty, U. Vaidya, H. Wang, V. Kunc, *Polym. Compos.* **2022**, *43*(6), 3678.
[67] N. Yousefi, M. M. Gudarzi, Q. Zheng, X. Lin, X. Shen, J. Jia, F. Sharif, J. K. Kim, *Compos. Part A Appl. Sci. Manuf.* **2013**, *49*, 42.
[68] S. U. Khan, J. R. Pothnis, J. K. Kim, *Compos. Part A Appl. Sci. Manuf.* **2013**, *49*, 26.
[69] G. Tan, J. Zhang, L. Zheng, D. Jiao, Z. Liu, Z. Zhang, R. O. Ritchie, *Adv. Mater.* **2019**, *31*(52), 1904603.
[70] H. Zhao, Y. Yue, L. Guo, J. Wu, Y. Zhang, X. Li, S. Mao, X. Han, *Adv. Mater.* **2016**, *28*(25), 5099.
[71] N. Burger, A. Laachachi, B. Mortazavi, M. Ferriol, M. Lutz, V. Toniazzo, D. Ruch, *Int. J. Heat Mass Transfer* **2015**, *89*, 505.
[72] J. Jing, Y. Chen, S. Shi, L. Yang, P. Lambin, *Chem. Eng. J.* **2020**, *402*, 126218.
[73] Z. Peng, L. Gong, J. Huang, Y. Wang, L. Tan, Y. Chen, *Carbon* **2019**, *153*, 531.
[74] T. A. Silva, H. Zanin, E. Saito, R. A. Medeiros, F. C. Vicentini, E. J. Corat, O. Fatibello-Filho, *Electrochim. Acta* **2014**, *119*, 114.
[75] S. Kim, J. R. Jinschek, H. Chen, D. S. Sholl, E. Marand, *Nano Lett.* **2007**, *7*(9), 2806.
[76] N. Hasanabadi, S. R. Ghaffarian, M. M. Hasani-Sadrabadi, *Int. J. Hydrogen Energy* **2011**, *36*(23), 15323.
[77] F. Besharat, M. Manteghian, F. Russo, F. Galiano, A. Figoli, M. Abdollahi, A. Lazzeri, *Polym. Adv. Technol.* **2021**, *32*(4), 1531.
[78] A. Chanda, S. K. Sinha, N. V. Datla, *Polym. Compos.* **2021**, *42*(3), 1155.
[79] M. Längauer, F. Brunnthaller, G. Zitzenbacher, C. Burgstaller, C. Hochenauer, *Polym. Compos.* **2021**, *42*(4), 2050.
[80] X. Luo, M. Qu, D. W. Schubert, *Polym. Compos.* **2021**, *42*(2), 548.
[81] S. Sharafkhani, M. Kokabi, *Compos. Sci. Technol.* **2020**, *200*, 108425.
[82] X. Wang, J. Jian, S. Diaz-Amaya, C. E. Kumah, P. Lu, J. Huang, D. G. Lim, V. G. Pol, J. P. Youngblood, A. Boltasseva, L. A. Stanciu, D. M. O'Carroll, X. Zhang, H. Wang, *Nanoscale Adv.* **2019**, *1*(3), 1045.
[83] H. Zhang, M. A. Marwat, B. Xie, M. Ashtar, K. Liu, Y. Zhu, L. Zhang, P. Fan, C. Samart, Z. G. Ye, *ACS Appl. Mater. Interfaces* **2020**, *12*(1), 1.
[84] H. Tang, Y. Lin, H. A. Sodano, *Adv. Energy Mater.* **2012**, *2*(4), 469.
[85] P. Singh, P. Singh, S. K. Shukla, *Dalton Trans.* **2020**, *49*(25), 8744.
[86] R. G. Suthar, B. Gao, *Water Purif.* **2017**, *3*, 75.
[87] J. Hu, S. Zhang, B. Tang, *Energy Storage Mater.* **2021**, *34*, 260.
[88] S. Giri, D. Ghosh, C. K. Das, *Adv. Funct. Mater.* **2014**, *24*(9), 1312.
[89] D. M. Cunha, M. Huijben, *MRS Bull.* **2021**, *46*(2), 152.

[90] Y. Liu, K. Wu, M. Lu, S. Nie, W. Chen, E. Jiao, B. Nan, L. Liang, M. Lu, *J. Mater. Sci.* **2020**, *55*(21), 8917.
[91] F. Guo, X. Shen, J. Zhou, D. Liu, Q. Zheng, J. Yang, B. Jia, A. K. T. Lau, J. K. Kim, *Adv. Funct. Mater.* **2020**, *30*(19), 1910826.
[92] M. Clausi, I. S. Bayer, *Nano Sel.* **2021**, *2*(2), 433.
[93] Q. Chen, Z. Ma, Z. Wang, L. Liu, M. Zhu, W. Lei, P. Song, *Adv. Funct. Mater.* **2022**, *32*(8), 2110782.
[94] L. Vaisman, E. Wachtel, H. D. Wagner, G. Marom, *Polymer (Guildf)* **2007**, *48*(23), 6843.
[95] S. Sinha Ray, M. Okamoto, *Prog. Polym. Sci.* **2003**, *28*(11), 1539.
[96] M. Okamoto, P. H. Nam, P. Maita, T. Kotaka, T. Nakayama, M. Takada, M. Ohshima, A. Usuki, N. Hasegawa, H. Okamoto, *Nano Lett.* **2001**, *1*(9), 503.
[97] M. Naebe, T. Lin, M. P. Staiger, L. Dai, X. Wang, *Nanotechnology* **2008**, *19*(30), 305702.
[98] C. M. Koo, J. H. Kim, K. I. H. Wang, I. N. J. Chung, *J. Polym. Sci. Part B Polym. Phys.* **2005**, *43*(2), 158.
[99] G. M. Lambert, P. Wapperom, D. Baird, *Polym. Compos.* **2021**, *42*(1), 98.
[100] S. Wu, J. Zhang, R. B. Ladani, K. Ghorbani, A. P. Mouritz, A. J. Kinloch, C. H. Wang, *Polymer (Guildf)* **2016**, *97*, 273.
[101] Chu, C. J.; Yeh, C. S. Sen; Liao, C. K.; Tsai, L. C.; Huang, C. M.; Lin, H. Y.; Shyue, J. J.; Chen, Y. T.; Chen, C. D. *Nano Lett.* **2013**, *13* (6), 2564–2569.
[102] S. I. Yun, D. Attard, V. Lo, J. Davis, H. Li, B. Latella, F. Tsvetkov, H. Noorman, S. Moricca, R. Knott, H. Hanley, M. Morcom, G. P. Simon, G. E. Gadd, *J. Appl. Polym. Sci.* **2008**, *108*(3), 1550.
[103] A. Thompson, O. Bianchi, C. L. G. Amorim, C. Lemos, S. R. Teixeira, D. Samios, C. Giacomelli, J. S. Crespo, G. MacHado, *Polymer (Guildf).* **2011**, *52*(4), 1037.
[104] X. Li, H. Yu, X. Kang, G. Chen, M. Zhu, J. Xu, *J. Appl. Polym. Sci.* **2021**, *138*(1), 49633.
[105] G. Wang, G. Zhao, S. Wang, L. Zhang, C. B. Park, *J. Mater. Chem. C* **2018**, *6*(25), 6847.
[106] X. Zhang, X. Li, Y. Ren, G. Yang, K. Ou, R. Guang, Y. Sun, *Iran. Polym. J.* **2022**, *2022*, 1.
[107] J. Zhan, J. Li, G. Wang, Y. Guan, G. Zhao, J. Lin, H. Naceur, D. Coutellier, *Polym. Compos.* **2021**, *42*(3), 1305.
[108] S. Pujari, W. R. Burghardt, S. S. Rahatekar, A. H. Windle, K. K. Koziol, *AIP Conf. Proc.* **2008**, *1027*(1), 806.
[109] W. E. Mahmoud, S. A. Al-Bluwi, *Sensors Actuat. A Phys.* **2020**, *313*, 112166.
[110] M. Bhasin, S. Wu, R. B. Ladani, A. J. Kinloch, C. H. Wang, A. P. Mouritz, *Int. J. Fatigue* **2018**, *113*, 88.
[111] M. Dong, J. Zhang, G. Hou, L. Liu, X. Qu, Y. Yu, C. Yuan, X. Wang, *Compos. Commun.* **2020**, *17*, 61.
[112] P. Jiang, M. J. McFarland, *J. Am. Chem. Soc.* **2004**, *126*(42), 13778.
[113] M. M. Shameem, S. M. Sasikanth, R. Annamalai, R. G. Raman, *Mater. Today Proc.* **2021**, *45*, 2536.
[114] H. Yang, P. Jiang, *Langmuir* **2010**, *26*(16), 13173.
[115] J. I. Park, D. K. Kim, J. Jang, I. M. Kang, H. Kim, J. Park, I. W. Nam, P. Lang, J. H. Bae, *Compos. Sci. Technol.* **2020**, *200*, 108471.
[116] M. Pasichnyk, J. Gaálová, P. Minarik, M. Václavíková, I. Melnyk, *Sci. Rep.* **2022**, *12*(1), 1.
[117] J. Zhang, B. Li, L. Wu, A. Wang, *Chem. Commun.* **2013**, *49*(98), 11509.
[118] C. Yu, J. Song, Z. Ma, J. Lu, W. Xing, M. Meng, J. Dai, Y. Yan, Y. Wu, *Chem. Eng. J.* **2022**, *427*, 131610.
[119] C. Sinturel, M. Vayer, F. Mahut, F. Bonnier, I. Chourpa, E. Munnier, *Colloids Surf. A Physicochem. Eng. Asp.* **2021**, *608*, 125591.
[120] P. J. Chen, T. J. Liu, P. Y. Wu, C. F. Tseng, C. M. Leu, *AIChE J.* **2010**, *56*(3), 790.
[121] R. D. Sudduth, C. Rogers, *J. Polym. Sci. Polym. Lett. Ed.* **1973**, *11*(10), 603.
[122] A. Liu, A. Walther, O. Ikkala, L. Belova, L. A. Berglund, *Biomacromolecules* **2011**, *12*(3), 633.
[123] S. Ansari, A. Kelarakis, L. Estevez, E. P. Giannelis, *Small* **2010**, *6*(2), 205.
[124] G. Guzman, S. S. Es-haghi, T. Nugay, M. Cakmak, *Adv. Healthc. Mater.* **2017**, *6*(3), 1600775.
[125] H. Y. Huang, T. C. Huang, T. C. Yeh, C. Y. Tsai, C. L. Lai, M. H. Tsai, J. M. Yeh, Y. C. Chou, *Polymer (Guildf)* **2011**, *52*(11), 2391.
[126] M. Frounchi, S. Dadbin, Z. Salehpour, M. Noferesti, *J. Membr. Sci.* **2006**, *282*, 142.
[127] J. Gaume, C. Taviot-Gueho, S. Cros, A. Rivaton, S. Thérias, J. L. Gardette, *Sol. Energy Mater. Sol. Cells* **2012**, *99*, 240.
[128] M. A. Paul, C. Delcourt, M. Alexandre, P. Degée, F. Monteverde, A. Rulmont, P. Dubois, *Macromol. Chem. Phys.* **2005**, *206*(4), 484.
[129] J. J. Kochumalayil, M. Bergenstråhle-Wohlert, S. Utsel, L. Wågberg, Q. Zhou, L. A. Berglund, *Biomacromolecules* **2013**, *14*(1), 84.
[130] O. Yucel, E. Unsal, J. Harvey, M. Graham, D. H. Jones, M. Cakmak, *J. Membr. Sci.* **2015**, *495*, 65.
[131] R. Herrera Alonso, L. Estevez, H. Lian, A. Kelarakis, E. P. Giannelis, *Polymer (Guildf)* **2009**, *50*(11), 2402.
[132] N. Yousefi, M. M. Gudarzi, Q. Zheng, S. H. Aboutalebi, F. Sharif, J. K. Kim, *J. Mater. Chem.* **2012**, *22*(25), 12709.
[133] G. Spiaggia, P. Taladriz-Blanco, D. Septiadi, R. D. Ortuso, A. Lee, V. Trappe, B. Rothen-Rutishauser, A. Petri-Fink, *ACS Appl. Bio Mater.* **2021**, *4*(12), 8316.
[134] L. Reid, W. Y. Hamad, *ACS Appl. Polym. Mater.* **2022**, *4*(1), 598.
[135] M. Núñez-Martínez, S. Arias, E. Quiñoá, R. Riguera, F. Freire, *Chem. Mater.* **2021**, *33*(12), 4805.
[136] C. Le Bourlais, L. Acar, H. Zia, P. A. Sado, T. Needham, R. Leverge, *Prog. Retin. Eye Res.* **1998**, *17*(1), 33.
[137] X. Huang, C. S. Brazel, *J. Control. Release* **2001**, *73*(2–3), 121.
[138] P. I. Lee, *J. Control. Release* **1985**, *2*, 277.
[139] Y. Kuang, C. Chen, J. Cheng, G. Pastel, T. Li, J. Song, F. Jiang, Y. Li, Y. Zhang, S. H. Jang, G. Chen, T. Li, L. Hu, *Extrem. Mech. Lett.* **2019**, *29*, 100463.
[140] H. Zeng, J. Wu, Y. Ma, Y. Ye, J. Liu, X. Li, Y. Wang, Y. Liao, X. Luo, X. Xie, Y. W. Mai, *ACS Appl. Mater. Interfaces* **2018**, *10*(48), 41690.
[141] Z. G. Wang, W. Liu, Y. H. Liu, Y. Ren, Y. P. Li, L. Zhou, J. Z. Xu, J. Lei, Z. M. Li, *Compos. Part B Eng.* **2020**, *180*, 107569.
[142] Y. Meyva-Zeybek, C. Kaynak, *J. Appl. Polym. Sci.* **2021**, *138*(16), 50246.
[143] R. L. Ceballos, C. von Bilderling, L. Guz, C. Bernal, L. Famá, *Carbohydr. Polym.* **2021**, *261*, 117871.
[144] M. C. Mistretta, L. Botta, M. Morreale, S. Rifici, M. Ceraulo, F. P. La Mantia, *Mater* **2018**, *11*, 613.
[145] B. Wu, J. Lyu, C. Peng, J. Liu, S. Xing, D. Jiang, S. Ju, M. K. Tiwari, *Colloids Surf. A Physicochem. Eng. Asp.* **2020**, *590*, 124533.

[146] H. Suherman, A. B. Sulong, J. Sahari, *Ceram. Int.* **2013**, *39*(2), 1277.

[147] F. A. Zhang, D. K. Lee, T. J. Pinnavaia, *Polymer (Guildf)* **2009**, *50*(20), 4768.

[148] A. Durmuş, M. Woo, A. Kaşgöz, C. W. Macosko, M. Tsapatsis, *Eur. Polym. J.* **2007**, *43*(9), 3737.

[149] A. Arora, V. Choudhary, D. K. Sharma, *J. Polym. Res.* **2010**, *18*(4), 843.

[150] B. Yalcin, M. Cakmak, *Polymer (Guildf)* **2004**, *45*(19), 6623.

[151] S. Ansari, E. P. Giannelis, *J. Polym. Sci. Part B Polym. Phys.* **2009**, *47*(9), 888.

[152] C. M. Lin, C. I. Weng, *Polym. Compos.* **1999**, *20*(1), 98.

[153] Y. Liang, Y. Guo, E. Wang, M. Cakmak, *Macromolecules* **2015**, *48*(7), 2299.

[154] L. Xie, X. Y. Lv, Z. J. Han, J. H. Ci, C. Q. Fang, P. G. Ren, *Polym.-Plast. Technol. Eng.* **2012**, *51*(12), 1251.

[155] O. C. Compton, S. Kim, C. Pierre, J. M. Torkelson, S. T. Nguyen, *Adv. Mater.* **2010**, *22*(42), 4759.

[156] M. Mahmoodi, Y. H. Lee, A. Mohamad, S. S. Park, *Polym. Eng. Sci.* **2015**, *55*(4), 753.

[157] K. Kalaitzidou, H. Fukushima, L. T. A. Drzal, *Mater* **2010**, *3*(2), 1089.

[158] S. Abbasi, P. J. Carreau, A. Derdouri, *Polymer (Guildf)* **2010**, *51*(4), 922.

[159] Z. Liu, J. Li, X. Liu, *ACS Appl. Mater. Interfaces* **2020**, *12*(5), 6503.

[160] N. Sun, J. Sun, X. Zeng, P. Chen, J. Qian, R. Xia, R. Sun, *Compos. Part A Appl. Sci. Manuf.* **2018**, *110*, 45.

[161] C. Yu, W. Gong, W. Tian, Q. Zhang, Y. Xu, Z. Lin, M. Hu, X. Fan, Y. Yao, *Compos. Sci. Technol.* **2018**, *160*, 199.

[162] V. B. Gupta, *Manuf. Fibre Technol.* **1997**, *4*, 67.

[163] M. Persson, G. S. Lorite, S. W. Cho, J. Tuukkanen, M. Skrifvars, *ACS Appl. Mater. Interfaces* **2013**, *5*(15), 6864.

[164] Z. Wang, C. W. Macosko, F. S. Bates, *ACS Appl. Mater. Interfaces* **2016**, *8*(1), 754.

[165] S. Chatterjee, F. A. Nüesch, B. T. T. Chu, *Chem. Phys. Lett.* **2013**, *557*, 92.

[166] M. M. Mahat, A. S. M. Sabere, J. Azizi, N. A. N. Amdan, *Emergent Mater.* **2021**, *4*(1), 279.

[167] S. Arora, A. Majumdar, A. Majumdar, *J. Ind. Text.* **2022**, 1. https://doi.org/10.1177/15280837211069869

[168] R. Haggenmueller, H. H. Gommans, A. G. Rinzler, J. E. Fischer, K. I. Winey, *Chem. Phys. Lett.* **2000**, *330*(3–4), 219.

[169] A. Redondo, S. Chatterjee, P. Brodard, L. S. T. J. Korley, C. Weder, I. Gunkel, U. Steiner, *Polymer* **2019**, *11*, 1912.

[170] A. Bachs-Herrera, O. Yousefzade, L. J. Del Valle, J. Puiggali, *Appl. Sci* **2021**, *11*, 1808.

[171] Y. Liu, S. Kumar, *ACS Appl. Mater. Interfaces* **2014**, *6*(9), 6069.

[172] T. D. Fornes, J. W. Baur, Y. Sabba, E. L. Thomas, *Polymer (Guildf)* **2006**, *47*(5), 1704.

[173] D. Fischer, P. Pötschke, H. Brünig, A. Janke, *Macromol. Symp.* **2005**, *230*(1), 167.

[174] W. Steinmann, S. Walter, T. Gries, G. Seide, G. Roth, *Text. Res. J.* **2012**, *82*(18), 1846.

[175] P. Pötschke, H. Brünig, A. Janke, D. Fischer, D. Jehnichen, *Polymer (Guildf)* **2005**, *46*(23), 10355.

[176] E. Nilsson, H. Oxfall, W. Wandelt, R. Rychwalski, B. Hagström, *J. Appl. Polym. Sci.* **2013**, *130*(4), 2579.

[177] M. Qu, F. Nilsson, Y. Qin, G. Yang, Y. Pan, X. Liu, G. Hernandez Rodriguez, J. Chen, C. Zhang, D. W. Schubert, *Compos. Sci. Technol.* **2017**, *150*, 24.

[178] W. Gao, H. Dong, H. Hou, H. Zhang, *Carbohydr. Polym.* **2012**, *88*(1), 321.

[179] Y. Wang, Q. Liu, Z. C. Zhen, J. L. Liu, R. M. Qiao, W. Q. He, *J. Appl. Polym. Sci.* **2021**, *138*(26), 50610.

[180] Y. Zhou, *Polym. Compos. Electr. Eng.* **2021**, 1. https://doi.org/10.1002/9781119719687

[181] E. Picard, A. Vermogen, J. F. Gérard, E. Espuche, *J. Membr. Sci.* **2007**, *292*(1–2), 133.

[182] A. Mirzadeh, M. Kokabi, *Eur. Polym. J.* **2007**, *43*(9), 3757.

[183] G. Carotenuto, S. De Nicola, M. Palomba, D. Pullini, A. Horsewell, T. W. Hansen, L. Nicolais, *Nanotechnology* **2012**, *23*(48), 485705.

[184] J. Li, L. Lai, L. Wu, S. J. Severtson, W. J. Wang, *ACS Sustainable Chem. Eng.* **2018**, *6*(5), 6654.

[185] B. Li, P. I. Xidas, E. Manias, *ACS Appl. Nano Mater.* **2018**, *1*(7), 3520.

[186] C. Bavatharani, E. Muthusankar, S. M. Wabaidur, Z. A. Alothman, K. M. Alsheetan, AL-Anazy, M. mana; Ragupathy, D., *Synth. Met.* **2021**, *271*, 116609.

[187] N. Rosman, W. N. Wan Salleh, M. R. Jamalludin, M. R. Adam, N. H. Ismail, J. Jaafar, Z. Harun, A. F. Ismail, *Mater. Today Proc.* **2021**, *46*, 1824.

[188] K. D. Patel, A. R. Padalhin, R. A. G. Franco, F. Verisqa, H. W. Kim, L. Nguyen, *Biomed. Appl. Electrospin. Electrospray.* **2021**, *1*, 3.

[189] X. L. Cai, T. T. Jiang, C. M. Qiao, B. W. Cheng, W. M. Kang, *Appl. Mech. Mater.* **2014**, *633–634*, 11.

[190] L. Sethuram, J. Thomas, A. Mukherjee, N. Chandrasekaran, *Mater. Adv.* **2021**, *2*(9), 2971.

[191] N. Joy, R. Anuraj, A. Viravalli, H. N. Dixit, S. Samavedi, *Chem. Eng. Sci.* **2021**, *230*, 116200.

[192] P. M. Silva, C. Prieto, C. C. P. Andrade, J. M. Lagarón, L. M. Pastrana, M. A. Coimbra, A. A. Vicente, M. A. Cerqueira, *Int. J. Biol. Macromol.* **2022**, *202*, 453.

[193] H. Gade, S. Nikam, G. G. Chase, D. H. Reneker, *Polymer (Guildf)* **2021**, *228*, 123902.

[194] B. Ghorani, N. Tucker, *Food Hydrocoll.* **2015**, *51*, 227.

[195] P. P. Vo, H. N. Doan, K. Kinashi, W. Sakai, N. Tsutsumi, D. P. Huynh, *Polymer* **2018**, *10*, 680.

[196] H. M. Ibrahim, A. Klingner, *Polym. Test.* **2020**, *90*, 106647.

[197] K. Zhao, S. X. Kang, Y. Y. Yang, D. G. Yu, *Polymer* **2021**, *13*, 226.

[198] C. L. Casper, J. S. Stephens, N. G. Tassi, D. B. Chase, J. F. Rabolt, *Macromolecules* **2003**, *37*(2), 573.

[199] S. De Vrieze, T. Van Camp, A. Nelvig, B. Hagström, P. Westbroek, K. De Clerck, *J. Mater. Sci.* **2009**, *44*(5), 1357.

[200] J. Pelipenko, J. Kristl, B. Janković, S. Baumgartner, P. Kocbek, *Int. J. Pharm.* **2013**, *456*(1), 125.

[201] L. Huang, N. N. Bui, S. S. Manickam, J. R. McCutcheon, *J. Polym. Sci. Part B Polym. Phys.* **2011**, *49*(24), 1734.

[202] Y. Ji, B. Li, S. Ge, J. C. Sokolov, M. H. Rafailovich, *Langmuir* **2006**, *22*(3), 1321.

[203] S. Cuenot, S. Demoustier-Champagne, B. Nysten, *Phys. Rev. Lett.* **2000**, *85*(8), 1690.

[204] Q. Zhang, Z. Chang, M. Zhu, X. Mo, D. Chen, Q. Zhang, Z. Chang, M. Zhu, X. Mo, D. Chen, *Nanotechnology* **2007**, *18*(11), 115611.

[205] K. Saeed, S. Y. Park, H. J. Lee, J. B. Baek, W. S. Huh, *Polymer (Guildf)* **2006**, *47*(23), 8019.

[206] K. Saeed, S. Y. Park, S. Haider, J. B. Baek, *Nanoscale Res. Lett.* **2009**, *4*(1), 39.
[207] M. S. Kang, M. K. Shin, Y. A. Ismail, S. R. Shin, S. I. Kim, H. Kim, H. Lee, S. J. Kim, *Nanotechnology* **2009**, *20*(8), 085701.
[208] J. Gao, M. E. Itkis, A. Yu, E. Bekyarova, B. Zhao, R. C. Haddon, *J. Am. Chem. Soc.* **2005**, *127*(11), 3847.
[209] S. Kedem, J. Schmidt, Y. Paz, Y. Cohen, *Langmuir* **2005**, *21*(12), 5600.
[210] H. Hou, J. J. Ge, J. Zeng, Q. Li, D. H. Reneker, A. Greiner, S. Z. D. Cheng, *Chem. Mater.* **2005**, *17*(5), 967.
[211] D. Chen, T. Liu, X. Zhou, W. C. Tjiu, H. Hou, *J. Phys. Chem. B* **2009**, *113*(29), 9741.
[212] B. Sundaray, V. Subramanian, T. S. Natarajan, K. Krishnamurthy, *Appl. Phys. Lett.* **2006**, *88*(14), 143114.
[213] L. Q. Liu, D. Tasis, M. Prato, H. D. Wagner, *Adv. Mater.* **2007**, *19*(9), 1228.
[214] K. K. H. Wong, M. Zinke-Allmang, J. L. Hutter, S. Hrapovic, J. H. T. Luong, W. Wan, *Carbon* **2009**, *47*(11), 2571.
[215] Y. Dror, W. Salalha, R. L. Khalfin, Y. Cohen, A. L. Yarin, E. Zussman, *Langmuir* **2003**, *19*(17), 7012.
[216] J. J. Ge, H. Hou, Q. Li, M. J. Graham, A. Greiner, D. H. Reneker, F. W. Harris, S. Z. D. Cheng, *J. Am. Chem. Soc.* **2004**, *126*(48), 15754.
[217] M. S. P. Shaffer, A. H. Windle, *Adv. Mater.* **1999**, *11*, 937.
[218] S. D. McCullen, D. R. Stevens, W. A. Roberts, S. S. Ojha, L. I. Clarke, R. E. Gorga, *Macromolecules* **2007**, *40*(4), 997.
[219] V. Datsyuk, S. Trotsenko, S. Reich, *Carbon* **2013**, *52*, 605.
[220] F. Peng, M. T. Shaw, J. R. Olson, M. Wei, *J. Phys. Chem. C* **2011**, *115*(32), 15743.
[221] P. P. Xu, S. Yang, X. R. Gao, S. P. Chen, L. Xu, G. J. Zhong, H. D. Huang, Z. M. Li, *Compos. Part B Eng.* **2021**, *222*, 109048.
[222] R.-C. Zhang, Z. Huang, M. Zhong, D. Ji, A. Lu, Q. Zhang, Y. Lin, P. Joseph, J. Zhang, D. Sun, R.-C. Zhang, Z. Huang, M. Zhong, D. Ji, Q. Zhang, J. Zhang, A. Lu, Y. Lin, P. Joseph, D. Sun, *Macromol. Mater. Eng.* **2022**, *307*(1), 2100695.
[223] Q. E. Wang, H. Niu, Y. Wang, C. Li, *Mol. Cryst. Liq. Cryst.* **2021**, *732*, 11.
[224] W. L. Song, W. Wang, L. M. Veca, C. Y. Kong, M. S. Cao, P. Wang, M. J. Meziani, H. Qian, G. E. Lecroy, L. Cao, Y. P. Sun, *J. Mater. Chem.* **2012**, *22*(33), 17133.
[225] F. You, X. Li, L. Zhang, D. Wang, C. Y. Shi, Z. M. Dang, *RSC Adv.* **2017**, *7*(10), 6170.
[226] X. Zhang, D. Xiang, Y. Wu, E. Harkin-Jones, J. Shen, Y. Ye, W. Tan, J. Wang, P. Wang, C. Zhao, Y. Li, *Compos. Part A Appl. Sci. Manuf.* **2021**, *151*, 106665.
[227] J. Yan, J. Yang, S. Dong, K. Huang, J. Ruan, J. Hu, H. Zhou, Q. Zhu, X. Zhang, Y. Ding, *Nanotechnology* **2019**, *30*(27), 275602.
[228] Y. Yang, J. Zhang, *Energy Storage Mater.* **2021**, *37*, 135.
[229] B. Xue, Z. Cheng, S. Yang, X. Sun, L. Xie, Q. Zheng, *Compos. Part B Eng.* **2021**, *207*, 108556.
[230] J. Férec, E. Bertevas, G. Ausias, N. Phan-Thien, *Flow-Induc. Alignm. Compos. Mater.* **2022**, *4*, 77.
[231] J. Lu, W. Weng, X. Chen, D. Wu, C. Wu, G. Chen, *Adv. Funct. Mater.* **2005**, *15*(8), 1358.
[232] C. Mao, J. Huang, Y. Zhu, W. Jiang, Q. Tang, X. Ma, *J. Phys. Chem. Lett.* **2013**, *4*(1), 43.
[233] J. Huang, Y. Zhu, W. Jiang, J. Yin, Q. Tang, X. Yang, *ACS Appl. Mater. Interfaces* **2014**, *6*(3), 1754.
[234] L. J. Lanticse, Y. Tanabe, K. Matsui, Y. Kaburagi, K. Suda, M. Hoteida, M. Endo, E. Yasuda, *Carbon* **2006**, *44*(14), 3078.
[235] E. D. Sapper, L. J. Brickweg, B. R. Floryancic, R. H. Fernando, *ACS Symp. Ser.* **2009**, *1008*, 108.
[236] G. Chen, Z. Qi, D. Shen, *J. Mater. Res.* **2000**, *15*(2), 351.
[237] J. R. Pothnis, D. Kalyanasundaram, S. Gururaja, *Compos. Part A Appl. Sci. Manuf.* **2021**, *149*, 106544.
[238] K. R. Park, H. B. Cho, M. Lim, B. K. Jang, J. Lee, B. S. Jeon, Y. H. Choa, *Appl. Surf. Sci.* **2021**, *551*, 149201.
[239] A. Kumar, K. Patra, M. Hossain, *Polym. Compos.* **2021**, *42*(2), 914.
[240] S. Jin, B. Zhang, X. Liu, B. Yang, R. Ge, Z. Qiang, Y. Chen, *J. Polym. Eng.* **2022**. https://doi.org/10.1515/polyeng-2022-0035
[241] C. Park, R. E. Robertson, *Mater. Sci. Eng. A* **1998**, *257*(2), 295.
[242] C. Park, J. Wilkinson, S. Banda, Z. Ounaies, K. E. Wise, G. Sauti, P. T. Lillehei, J. S. Harrison, *J. Polym. Sci. Part B Polym. Phys.* **2006**, *44*(12), 1751.
[243] T. Prasse, J. Y. Cavaillé, W. Bauhofer, *Compos. Sci. Technol.* **2003**, *13*(63), 1835.
[244] D. A. Norman, R. E. Robertson, *J. Appl. Polym. Sci.* **2003**, *90*(10), 2740.
[245] S. Batra, E. Unsal, M. Cakmak, *Adv. Funct. Mater.* **2014**, *24*(48), 7698.
[246] B. Yalcin, M. Cakmak, *J. Polym. Sci. Part B Polym. Phys.* **2005**, *43*(6), 724.
[247] S. Kitajima, M. Matsuda, M. Yamato, Y. Tominaga, *Polym. J.* **2013**, *45*(7), 738.
[248] P. Aranda, E. Ruiz-Hitzky, *Chem. Mater.* **2002**, *4*(6), 1395.
[249] C. P. Bowen, R. E. Newnham, C. A. Randall, *J. Mater. Res.* **1998**, *13*(1), 205.
[250] Y. Guo, S. Batra, Y. Chen, E. Wang, M. Cakmak, *ACS Appl. Mater. Interfaces* **2016**, *8*(28), 18471.
[251] M. Knaapila, O. T. Rømoen, E. Svasand, J. P. Pinheiro, Ø. G. Martinsen, M. Buchanan, A. T. Skjeltorp, G. Helgesen, *ACS Appl. Mater. Interfaces* **2011**, *3*(2), 378.
[252] H. B. Cho, A. Konno, T. Fujihara, T. Suzuki, S. Tanaka, W. Jiang, H. Suematsu, K. Niihara, T. Nakayama, *Compos. Sci. Technol.* **2011**, *72*(1), 112.
[253] Y. Guo, Y. Chen, E. Wang, M. Cakmak, *ACS Appl. Mater. Interfaces* **2017**, *9*(1), 919.
[254] Z. Han, J. Wang, Q. You, X. Liu, B. Xiao, Z. Liu, J. Liu, Y. Chen, *Polymers (Basel)* **2021**, *13*(21), 3826.
[255] Y. Chen, Y. Liu, Y. Xia, X. Liu, Z. Qiang, J. Yang, B. Zhang, Z. Hu, Q. Wang, W. Wu, Y. Duan, K. K. Fu, J. Zhang, *ACS Appl. Mater. Interfaces* **2020**, *12*(21), 24242.
[256] W. Wu, X. Liu, Z. Qiang, J. Yang, Y. Liu, K. Huai, B. Zhang, S. Jin, Y. Xia, K. K. Fu, J. Zhang, Y. Chen, *Compos. Sci. Technol.* **2021**, *216*, 109070.
[257] S. Jin, T. H. Tiefel, R. Wolfe, *IEEE Trans. Magn.* **1992**, *28*(5), 2211.
[258] M. Knaapila, H. Høyer, J. Kjelstrup-Hansen, G. Helgesen, *ACS Appl. Mater. Interfaces* **2014**, *6*(5), 3469.
[259] E. Breval, M. Klimkiewicz, Y. T. Shi, D. Arakaki, J. P. Dougherty, *J. Mater. Sci.* **2003**, *38*(6), 1347.
[260] H. Niu, Q. Chen, H. Zhu, Y. Lin, X. Zhang, *J. Mater. Chem.* **2003**, *13*(7), 1803.
[261] A. Anwer, A. H. Windle, *Polymer (Guildf)* **1993**, *34*(16), 3347.
[262] M. Gopinadhan, P. W. Majewski, E. S. Beach, C. O. Osuji, *ACS Macro Lett.* **2012**, *1*(1), 184.

[263] C. Osuji, P. J. Ferreira, G. Mao, C. K. Ober, J. B. V. Sande, E. L. Thomas, *Macromolecules* **2004**, *37*(26), 9903.
[264] T. Pullawan, A. N. Wilkinson, S. J. Eichhorn, *Biomacromolecules* **2012**, *13*(8), 2528.
[265] E. S. Choi, J. S. Brooks, D. L. Eaton, M. S. Al-Haik, M. Y. Hussaini, H. Garmestani, D. Li, K. Dahmen, *J. Appl. Phys.* **2003**, *94*(9), 6034.
[266] J. Liu, S. Z. Qiao, Q. H. Hu, G. Q. Lu, *Small* **2011**, *7*(4), 425.
[267] S. Zhang, C. I. Pelligra, X. Feng, C. O. Osuji, *Adv. Mater.* **2018**, *30*(18), 1705794.
[268] A. Sierra-Romero, B. Chen, *Nano* **2018**, *4*(4), 137.
[269] M. Gao, Y. Yang, W. F. Rao, D. Viehland, *MRS Bull.* **2021**, *46*(2), 123.
[270] D. M. Schaetzl, P. Li, N. Chaudhari, G. H. Bernstein, S. K. Fullerton-Shirey, *J. Phys. Chem. C* **2014**, *118*(33), 18836.
[271] B. W. Steinert, D. R. Dean, *Polymer (Guildf)* **2009**, *50*(3), 898.
[272] J. Billaud, F. Bouville, T. Magrini, C. Villevieille, A. R. Studart, *Nat. Energy* **2016**, *18*, 1.
[273] L. Cao, Z. Cheng, M. Yan, Y. Chen, *Chem. Eng. J.* **2019**, *363*, 203.
[274] D. Yao, N. Peng, Y. Zheng, *Compos. Sci. Technol.* **2018**, *167*, 234.
[275] M. Chaichi, F. Sharif, S. Mazinani, *J. Mater. Sci.* **2017**, *53*(7), 5051.
[276] D. Liu, H. Chi, C. Ma, M. Song, P. Zhang, P. Dai, *Compos. Sci. Technol.* **2022**, *220*, 109292.
[277] A. P. S. Zanatta, T. S. Daitx, L. N. Carli, C. S. Teixeira, R. S. Mauler, *J. Magn. Magn. Mater.* **2022**, *549*, 169015.
[278] Y. Chen, Y. Guo, S. Batra, E. Wang, Y. Wang, X. Liu, Y. Wang, M. Cakmak, *Nanoscale* **2015**, *7*(35), 14636.
[279] Y. Chen, Y. Guo, S. Batra, E. Unsal, E. Wang, Y. Wang, X. Liu, Y. Wang, M. Cakmak, *RSC Adv.* **2015**, *5*(112), 92071.
[280] M. Cakmak, S. Batra, B. Yalcin, *Polym. Eng. Sci.* **2015**, *55*(1), 34.
[281] S. A. M. Tofail, E. P. Koumoulos, A. Bandyopadhyay, S. Bose, L. O'Donoghue, C. Charitidis, *Mater. Today* **2018**, *21*(1), 22.
[282] M. Bhuvanesh Kumar, P. Sathiya, *Thin-Walled Struct.* **2021**, *159*, 107228.
[283] M. Sauerwein, E. Doubrovski, R. Balkenende, C. Bakker, *J. Clean. Prod.* **2019**, *226*, 1138.
[284] A. Borkar, A. Hendlmeier, Z. Simon, J. D. Randall, F. Stojcevski, L. C. Henderson, *Polym. Compos.* **2022**, *43*(4), 2408.
[285] M. A. Rahman, M. Z. Islam, L. Gibbon, C. A. Ulven, J. J. La Scala, *Polym. Compos.* **2021**, *42*(11), 5859.
[286] Q. Wang, X. Liu, Z. Qiang, Z. Hu, X. Cui, H. Wei, J. Hu, Y. Xia, S. Huang, J. Zhang, K. Fu, (Kelvin); Chen, Y., *Compos. Sci. Technol.* **2022**, *227*, 109601.
[287] Y. Yuan, H. Hu, W. Wu, Z. Zhao, X. Du, Z. Wang, *Polym. Compos.* **2021**, *42*(8), 4105.
[288] M. Delic, D. R. Eyers, *Int. J. Prod. Econ.* **2020**, *228*, 107689.
[289] A. A. Alogla, M. Baumers, C. Tuck, W. Elmadih, *Appl. Sci* **2021**, *11*, 3707.
[290] I. Gibson, D. Rosen, B. Stucker, M. Khorasani, *Addit. Manuf. Technol.* **2021**, *19*, 555.
[291] Z. Hu, Y. Wang, X. Liu, Q. Wang, X. Cui, S. Jin, B. Yang, Y. Xia, S. Huang, Z. Qiang, K. Fu, J. Zhang, Y. Chen, *Compos. Sci. Technol.* **2022**, *223*, 109403.
[292] L. J. Tan, W. Zhu, K. Zhou, *Adv. Funct. Mater.* **2020**, *30*(43), 2003062.
[293] G. Liu, X. Zhang, X. Chen, Y. He, L. Cheng, M. Huo, J. Yin, F. Hao, S. Chen, P. Wang, S. Yi, L. Wan, Z. Mao, Z. Chen, X. Wang, Z. Cao, J. Lu, *Mater. Sci. Eng. R Rep.* **2021**, *145*, 100596.
[294] T. Peng, K. Kellens, R. Tang, C. Chen, G. Chen, *Addit. Manuf.* **2018**, *21*, 694.
[295] C. Gao, S. Wolff, S. Wang, *J. Manuf. Syst.* **2021**, *60*, 459.
[296] C. Prakash, S. Singh, H. Kopperi, S. Ramakrihna, S. V. Mohan, *J. Clean. Prod.* **2021**, *289*, 125164.
[297] A. Ghobadian, I. Talavera, A. Bhattacharya, V. Kumar, J. A. Garza-Reyes, N. O'Regan, *Int. J. Prod. Econ.* **2020**, *219*, 457.
[298] J. Jiang, X. Xu, J. Stringer, *Robot. Comput. Integr. Manuf.* **2019**, *59*, 317.
[299] V. Shanmugam, O. Das, R. E. Neisiany, K. Babu, S. Singh, M. S. Hedenqvist, F. Berto, S. Ramakrishna, *Mater. Circ. Econ.* **2020**, *21*(1), 1.
[300] L. Bourdon, J. C. Maurin, K. Gritsch, A. Brioude, V. Salles, *ACS Biomater Sci. Eng.* **2018**, *4*(12), 3927.
[301] K. Zhang, G. Cheng, *Addit. Manuf.* **2020**, *35*, 101224.
[302] E. Jabari, F. Liravi, E. Davoodi, L. Lin, E. Toyserkani, *Addit. Manuf.* **2020**, *35*, 101330.
[303] G. Sabiston, I. Y. Kim, *Struct. Multidiscip. Optim.* **2019**, *61*(2), 731.
[304] D. Behera, S. Chizari, L. A. Shaw, M. Porter, R. Hensleigh, Z. Xu, N. K. Roy, L. G. Connolly, X. Zheng, S. Saha, J. B. Hopkins, M. A. Cullinan, *Precis. Eng.* **2021**, *68*, 301.
[305] A. Lalehpour, A. Barari, *Int. J. Adv. Manuf. Technol.* **2017**, *96*(9), 3793.
[306] P. Fiedor, J. Ortyl, *Mater* **2020**, *13*, 2951.
[307] E. A. Guzzi, M. W. Tibbitt, *Adv. Mater.* **2020**, *32*(13), 1901994.
[308] W. Xu, S. Jambhulkar, D. Ravichandran, Y. Zhu, M. Kakarla, Q. Nian, B. Azeredo, X. Chen, K. Jin, B. Vernon, D. G. Lott, J. L. Cornella, O. Shefi, G. Miquelard-Garnier, Y. Yang, K. Song, *Small* **2021**, *17*(45), 2100817.

How to cite this article: A. Griffin, Y. Guo, Z. Hu, J. Zhang, Y. Chen, Z. Qiang, *Polym. Compos.* **2022**, *43*(9), 5747. https://doi.org/10.1002/pc.26905